Iranian Journal of Basic Medical Sciences
ijbms.mums.ac.ir

Development and characterization of a saponin-stabilized berberine-loaded nanoemulgel for topical delivery

Ebru Altuntaş [1]*, Zakaria Ouzaid [1, 2], Aslı Gürbüz Yurtsever [1]

[1] Department of Pharmaceutical Technology, Faculty of Pharmacy, Istanbul University, Istanbul, Türkiye
[2] Graduate School of Health Sciences, Istanbul University, Istanbul, Türkiye

ARTICLE INFO

Article type:
Original

Article history:
Received: Jul 30, 2026
Accepted: Nov 1, 2026

Keywords:
Cell migration
Drug delivery systems
Keratinocytes
Nanoemulsion
Skin permeation
Xanthan gum

ABSTRACT

Objective(s): Berberine chloride has been investigated for topical wound applications; however, insufficient skin permeability and local availability may limit its local cutaneous delivery. This study aimed to develop and characterize a berberine-loaded nanoemulgel to modulate drug release and improve topical delivery.

Materials and Methods: Berberine-loaded nanoemulsions were prepared by ultrasonication and characterized for droplet size, polydispersity index, zeta potential, pH, conductivity, and stability. The optimized nanoemulsion was incorporated into xanthan gum hydrogel and evaluated for texture, spreadability, and three-month stability. *In vitro* release, *ex vivo* skin permeation and deposition, HaCaT cytocompatibility, and scratch-closure assays were performed.

Results: NEJ1.3 exhibited nanoscale droplets, a narrow size distribution, and satisfactory physicochemical stability. At 24 hr, the nanoemulgel showed sustained berberine release (63.22±2.25%) and the highest mean skin deposition (44.0[illegible]4±6.365 µg/cm²), whereas the nanoemulsion showed the highest mean permeation. Cell viability remained ≥70% across all formulations up to 12.5 mg/ml. The nanoemulgel produced significantly greater in vitro scratch closure than free berberine after 24 hr (76.33±3.43% vs. 25.56±4.29%, P<0.0001).

Conclusion: The berberine-loaded nanoemulgel provided sustained drug release, high skin deposition, acceptable cytocompatibility, and significantly greater *in vitro* scratch closure than free berberine. These findings support its potential as a topical berberine delivery system and warrant further *in vivo* evaluation.

▶Please cite this article as:
Altuntaş E, Ouzaid Z, Yurtsever AG. Development and characterization of a saponin-stabilized berberine-loaded nanoemulgel for topical delivery. Iran J Basic Med Sci 2027; 30:

Corrected Proof

Introduction

Wound healing is a multifaceted biological process comprising several overlapping stages, including hemostasis, inflammation, proliferation, and remodeling (1). Effective topical wound management requires formulation strategies that support local delivery of therapeutic agents while maintaining appropriate contact with the wound environment (2). Plant-derived compounds have attracted increasing interest in wound-related topical formulations because of their diverse biological activities and potential roles in tissue repair (3). Berberine, an isoquinoline alkaloid found in several medicinal plants, including Berberis species, has been investigated in experimental wound-related delivery systems, including nanofibrous dressings and lecithin–chitosan nanoparticles, providing a basis for further evaluation in topical formulations (4, 5). Berberine chloride, the salt form used in the present study, is more water-soluble than the corresponding free base, which facilitates its incorporation into aqueous pharmaceutical systems. Nevertheless, aqueous solubility alone does not ensure efficient topical delivery across the skin's highly organized barrier. Limited cutaneous penetration and low bioavailability may restrict berberine's local availability at the intended site of action (6). Therefore, the principal formulation challenge addressed in the present study is not simply aqueous solubilization, but developing a topical carrier that modulates drug release, improves drug–skin interaction, and promotes local cutaneous delivery.

Nanoemulsion-based systems represent a potential strategy for addressing the topical delivery limitations of berberine chloride. Although conventional hydrogels provide favorable viscosity, spreadability, and residence at the application site, they lack a dispersed nanoscale lipid phase and therefore offer limited opportunities to modulate drug partitioning and drug–skin interactions. Nanoemulsions, in contrast, provide a large interfacial area through their nanoscale droplets, while their oil phase and interfacial components can influence drug partitioning, contact with the skin surface, and transport across the cutaneous barrier (7, 8). Their composition can also be adjusted to modulate drug release and local skin distribution. Other lipid-based nanocarriers, including liposomes, solid lipid nanoparticles (SLNs), and nanostructured lipid carriers (NLCs), also represent valuable approaches for topical drug

***Corresponding author:** Ebru Altuntaş. Department of Pharmaceutical Technology, Faculty of Pharmacy, Istanbul University, Istanbul, Türkiye. Tel/ Fax: +90-212 4400252, Email: ebru.altuntas@istanbul.edu.tr

© 2027. This work is openly licensed via CC BY 4.0.
This is an Open Access article distributed under the terms of the Creative Commons Attribution License (https://creativecommons.org/licenses), which permits unrestricted use, distribution, and reproduction in any medium, provided the original work is properly cited.

delivery. However, these systems involve different structural architectures and formulation requirements, including vesicular bilayers or solid/semi-solid lipid matrices. In the present study, an oil-in-water nanoemulsion was selected as a comparatively simple liquid-dispersed system that enabled incorporation of Quillaja saponaria saponins (QSS) as a natural biosurfactant and subsequent direct incorporation of the nanoscale dispersion into a xanthan gum hydrogel. This nanoemulsion-to-nanoemulgel approach was therefore intended to combine droplet-mediated modulation of berberine partitioning and release with the viscosity, spreadability, and prolonged surface residence provided by the hydrogel matrix. Accordingly, the rationale for selecting the nanoemulsion was related primarily to its potential to modulate topical drug delivery rather than to overcome poor aqueous solubility of berberine chloride. Accordingly, for berberine chloride, the nanoemulsion was investigated not primarily as a solubilizing system, but as a carrier capable of modulating drug release, drug partitioning, and local cutaneous distribution after topical application. Nanoemulsion-based systems may also provide sustained drug release, which can be advantageous when prolonged local drug exposure is desired (9).

Saponins are naturally occurring amphiphilic glycosides that have attracted increasing interest as biosurfactants because of their surface-active properties and ability to stabilize dispersed systems (10). QSS, obtained from the bark of *Quillaja saponaria*, has a molecular structure with hydrophobic and hydrophilic domains that enable adsorption at the oil–water interface and stabilization of emulsion droplets (11-13). QSS have consequently been investigated as natural emulsifiers for nanoemulsion-based delivery systems, providing an alternative to conventional synthetic surfactants (12, 13). This characteristic is particularly relevant to topical formulation design, where surfactant selection influences droplet formation, colloidal stability, and formulation interaction with the application site. Therefore, QSS were selected in the present study primarily for their role as natural biosurfactants that stabilize the berberine-loaded nanoemulsion.

Converting nanoemulsions into nanoemulgels improves viscosity, application characteristics, and residence time at the skin surface while retaining the drug-delivery advantages of the dispersed nanosystem (14, 15). Consequently, researchers have investigated nanoemulgels as topical wound-healing platforms for several bioactive compounds (16-18). Researchers have also studied berberine in other topical and wound-oriented carriers, including a transfersomal emulgel, nanofibrous dressings, and lecithin–chitosan nanoparticles (4-6). These studies support investigation of berberine delivery systems but do not establish the release, skin-distribution, or cellular-response profile of the QSS-stabilized, xanthan gum-based formulation examined here.

This study examines a combination of a berberine chloride-loaded nanoemulsion stabilized with *Q. saponaria* saponins and a xanthan gum gel matrix. It jointly assesses formulation stability, mechanical properties, drug release, skin permeation and deposition, and HaCaT cell responses within this specific system. Comparison with a conventional berberine gel provides context for interpreting formulation-dependent differences in release and skin delivery.

This study aimed to develop and characterize a QSS-stabilized, berberine-loaded nanoemulgel and to evaluate its topical delivery properties and initial responses in a keratinocyte model relevant to wound repair. In this context, the designed nanoemulsion formulations were prepared using ultrasonic emulsification. QSS were selected as the natural biosurfactant to stabilize the nanoemulsion droplets, consistent with their previously reported use in oil-in-water nanoemulsions (13, 19). The prepared nanoemulsion formulations were evaluated for droplet size, polydispersity index (PDI), and zeta potential before and after accelerated stability tests (thermal and centrifugation tests). The most suitable formulations were then mixed with a natural polymeric gel containing xanthan gum at a specific ratio to form the nanoemulgel. After completing the characterization studies and accelerated stability tests of the prepared nanoemulgels, physicochemical stability, *in vitro* release, and *ex vivo* penetration studies were conducted with the optimized nanoemulgel formulation. Finally, HaCaT cytocompatibility and *in vitro* scratch assays were performed to assess cell viability and cell-layer closure under the tested conditions.

Materials and Methods

Materials

Berberine, QSS (catalog no. S4521-25G), and DL-α-tocopheryl acetate were purchased from Sigma-Aldrich (St. Louis, MO, USA). Xanthan gum (Vanzan® NF-C) was obtained from Vanderbilt Minerals, LLC (Norwalk, CT, USA). Caprylic/capric triglyceride (Crodamol™ GTCC) was kindly supplied by Croda (Snaith, UK). Diethylene glycol monoethyl ether (Transcutol® HP) was obtained from Gattefossé (Saint-Priest, France). Sensiva® PA 30 was kindly supplied by Schülke & Mayr GmbH (Norderstedt, Germany).

High-performance liquid chromatography (HPLC)-grade methanol, HPLC-grade acetonitrile, trifluoroacetic acid (TFA), and triethylamine were purchased from Merck (Darmstadt, Germany). Chromatographic analyses were performed using a Hypersil ODS-2 C18 column (250 × 4.6 mm, 5 µm; Thermo Fisher Scientific, Waltham, MA, USA). The mobile phase was filtered through 0.45 µm cellulose acetate membrane filters (ISOLAB, Eschau, Germany), and sample solutions were filtered through 0.45 µm polytetrafluoroethylene (PTFE) syringe filters (ISOLAB, Eschau, Germany) before HPLC analysis. Ultrapure water was obtained using a Milli-Q water purification system (Millipore, Bedford, MA, USA).

Spectra/Por® dialysis tubing cellulose membranes (molecular weight cut-off 12,000-14,000 Da; Spectrum Laboratories Inc., Rancho Dominguez, CA, USA) were used for the *in vitro* release studies. Fresh porcine ear skin obtained from a local slaughterhouse was used for the *ex vivo* permeation experiments.

The HaCaT cell line was obtained from Thermo Fisher Scientific (Waltham, MA, USA). Dulbecco's Modified Eagle's Medium (DMEM) was purchased from Sigma-Aldrich (St. Louis, MO, USA). Trypsin/EDTA (0.25%) was obtained from Gibco (Thermo Fisher Scientific, Waltham, MA, USA). Fetal bovine serum (FBS) and penicillin-streptomycin solution were purchased from Biological Industries (Beit HaEmek, Israel). MTT reagent was purchased from Biomatics (New Taipei City, Taiwan). All other chemicals and reagents were of analytical grade and used without further purification.

Corrected Proof

Preparation of berberine-loaded nanoemulsions

Berberine-loaded oil-in-water (O/W) nanoemulsions were developed using a high-energy ultrasonication technique (20). Six formulations were designed to investigate how biosurfactant concentration and berberine loading affect the physicochemical characteristics of the nanoemulsion system. The compositions of all formulations are presented in Table 1.

The oil phase consisted of caprylic/capric triglyceride as the carrier oil, DL-α-tocopherol acetate as an antioxidant, Sensiva® PA 30 as the preservative system, and Transcutol® HP as the co-surfactant. The aqueous phase contained berberine and QSS as a natural biosurfactant, and purified water served as the continuous phase. The berberine concentration was evaluated at two different levels (0.5% and 1.0%, w/w), whereas the concentration of QSS was varied between 5%, 7%, and 10% (w/w) to determine its effect on nanoemulsion formation and stability.

First, the oil-phase components were mixed until a homogeneous solution formed. In parallel, berberine and QSS were dissolved in the aqueous phase under magnetic stirring. The oil phase was then slowly added to the aqueous phase with continuous stirring to obtain a coarse emulsion.

Subsequently, the coarse emulsion was ultrasonicated using a probe-type ultrasonic homogenizer (20 kHz, 750 W). Ultrasonication was performed at 50% amplitude for 10 min under pulsed conditions (30 sec on/30 sec off). To prevent excessive temperature increases during emulsification and preserve the formulation's physicochemical stability, the sample vessel was immersed in an external ice bath throughout sonication.

After preparation, the nanoemulsions were initially characterized for mean droplet size, PDI, and zeta potential. Thereafter, accelerated stability studies, including centrifugation and thermal stress tests, were performed to assess their physical stability. Based on these initial characterization and stability results, the most suitable nanoemulsion formulations were selected for nanoemulgel preparation.

Characterization of nanoemulsion

Droplet size, PDI and zeta potential

The mean droplet size, PDI, and zeta potential of the freshly prepared nanoemulsions were determined using a Zetasizer Nano ZS (Malvern Panalytical Ltd., Malvern, UK), operating on the principles of dynamic light scattering (DLS) and electrophoretic light scattering (21). Before analysis, the nanoemulsions were diluted 1:100 (v/v) with ultrapure water to minimize multiple scattering effects (22). Measurements were performed at 25±0.5 ˚C using a fixed backscattering angle of 173˚. Zeta potential measurements were carried out using disposable folded capillary cells according to the manufacturer's instructions. Measurements were performed using three independently prepared samples (n=3), and the results were expressed as mean±SD.

Table 1. Composition of the developed berberine-loaded nanoemulsion formulations (%, w/w)

Component	0.5% Berberine			1.0% Berberine		
	NE1.1	NE1.2	NE1.3	NE2.1	NE2.2	NE2.3
Oil phase						
DL-α-Tocopheryl acetate	0.2	0.2	0.2	0.2	0.2	0.2
Caprylic/capric triglyceride	12.8	12.8	12.8	12.8	12.8	12.8
Sensiva® PA 30	2.0	2.0	2.0	2.0	2.0	2.0
Transcutol® HP	2.5	2.5	2.5	2.5	2.5	2.5
Aqueous phase						
Berberine	0.5	0.5	0.5	1.0	1.0	1.0
QSS	5.0	7.0	10.0	5.0	7.0	10.0
Purified water	77.0	75.0	72.0	76.5	74.5	71.5

NE = nanoemulsion; QSS = Quillaja saponaria saponins

Morphological analysis by transmission electron microscopy (TEM)

The morphology of the dispersed droplets in the selected BER-loaded nanoemulsion (NE1.3) was examined using a JEM-2100 Plus transmission electron microscope (TEM). The nanoemulsion was diluted 1:90 with distilled water, and an aliquot was placed on a copper grid. The sample was allowed to adsorb onto the grid for 10 min, after which excess sample was carefully removed using filter paper. Before the sample dried completely, 20 µl of uranyl acetate alternative staining solution was applied to the grid and left for 1 min. Excess staining solution was then removed, and the grid was allowed to dry completely before TEM examination. Images were acquired at an accelerating voltage of 80 kV.

Accelerated stability tests

The preliminary physical stability of the nanoemulsion formulations was evaluated by centrifugation and thermal stress testing (23, 24).

For the centrifugation test, the nanoemulsion samples were centrifuged at 3,500 rpm for 30 min. After centrifugation, the formulations were visually inspected for phase separation, creaming, sedimentation, or other macroscopic signs of instability. The mean droplet size, PDI, and zeta potential were then measured to evaluate the effect of centrifugal stress on the colloidal properties of the nanoemulsions.

For the thermal stress test, 5 g of each nanoemulsion formulation was transferred into glass tubes and exposed to temperatures ranging from 40 ˚C to 80 ˚C, in 5 ˚C increments, for 30 min at each temperature using a thermostatically controlled water bath (Witeg WSB-30, Germany). After completing the thermal stress protocol (80 ˚C), the formulations were visually examined for evidence of physical instability, after which the mean droplet size, PDI, and zeta potential were remeasured to assess the effect of thermal stress on the physicochemical characteristics of the nanoemulsions.

Preparation of berberine-loaded nanoemulgels

Nanoemulgels were prepared by incorporating the selected berberine-loaded nanoemulsions into xanthan gum hydrogels. Xanthan gum was evaluated at two different concentrations (1% and 2%, w/w) to investigate its suitability as a gelling agent.

Briefly, xanthan gum was gradually dispersed in ultrapure water under continuous magnetic stirring until a homogeneous hydrogel was obtained. The prepared hydrogel was then combined with the selected nanoemulsions at a 2:1 (w/w) nanoemulsion-to-hydrogel ratio and mixed gently

Corrected Proof

to form uniform nanoemulgels. This ratio maximized nanoemulsion content while minimizing berberine dilution in the final formulation.

Nanoemulgels were prepared only from the nanoemulsion formulations containing 0.5% (w/w) berberine. Three nanoemulsion formulations were combined with xanthan gum hydrogels containing either 1% or 2% (w/w) xanthan gum, yielding a total of six nanoemulgel formulations.

Characterization of nanoemulgels

Droplet size, polydispersity index (PDI), and zeta potential

The mean droplet size, PDI, and zeta potential of the nanoemulgel formulations were determined using the same instrument and experimental conditions described for the nanoemulsions (21). Before measurement, the nanoemulgel samples were diluted 1:100 (v/v) with ultrapure water to ensure adequate dispersion of the nanoemulsion droplets within the gel matrix (22). Measurements were performed using three independently prepared samples (n=3), and the results were expressed as mean±SD.

pH and conductivity measurements

The pH and electrical conductivity of the optimized nanoemulgel formulation were measured using a calibrated Hanna Edge multiparameter meter (Hanna Instruments, USA). Before analysis, the formulation was equilibrated to room temperature, and both measurements were performed directly on the sample without dilution. Each measurement was carried out in triplicate, and the results were expressed as mean±SD.

Rheological characterization

The rheological behavior of the optimized nanoemulgel formulation was evaluated using a Brookfield cone-and-plate viscometer (Brookfield Engineering Laboratories, Middleboro, MA, USA) equipped with a CP-40 spindle. Measurements were performed at 25±0.5 ˚C over a rotational speed range of 10-100 rpm. The corresponding viscosity and shear stress values were recorded at each rotational speed to characterize the flow behavior of the formulation. Rheological data were fitted to the Power Law model to determine the consistency index (K) and flow behavior index (n), and the coefficient of determination (R^2) was calculated to evaluate the goodness of fit.

Mechanical Characterization

Texture profile analysis (TPA)

The mechanical properties of the optimized berberine-loaded nanoemulgel and the conventional berberine gel were evaluated using a TA.XT Plus Texture Analyzer (Stable Micro Systems, Surrey, UK) (25). Before analysis, the gel samples were transferred to 25 ml glass beakers, and entrapped air bubbles were removed by placing the samples in an ultrasonic water bath.

TPA was performed using a P/0.75S (¾-inch spherical probe). Each sample underwent a two-cycle compression test with a 15 sec interval between compressions. The probe penetrated the gel to a depth of 15 mm at a test speed of 2 mm/sec, with a trigger force of 0.02 N. Measurements were performed in triplicate. The force-time curves were used to calculate hardness, adhesiveness, cohesiveness, springiness, and resilience.

Spreadability analysis

The spreadability of the optimized berberine-loaded nanoemulgel and the conventional berberine gel was evaluated using the same TA.XT Plus Texture Analyzer (Stable Micro Systems, Surrey, UK), equipped with a spreadability rig consisting of matched male and female conical probes (26).

Before analysis, the upper cone was calibrated at 23 mm. Gel samples were carefully transferred into the lower cone using a spatula, avoiding air entrapment and ensuring a smooth sample surface. During the test, the upper cone moved downward to a distance of 23 mm at a test speed of 3 mm/sec, followed by a post-test speed of 10 mm/sec. Measurements were performed in triplicate. The force-time curves were analyzed to determine firmness and the work of shear, which was used as an indicator of spreadability.

HPLC analysis and method validation

Berberine concentrations in all formulation, release, permeation, and drug content studies were determined using a validated reverse-phase RP-HPLC method adapted from a previously reported procedure with minor modifications (27). Chromatographic analyses were performed using an HPLC system equipped with a photodiode array (PDA) detector. Separation was achieved on a Hypersil ODS-2 C18 column (250×4.6 mm, 5 µm; Thermo Fisher Scientific, USA). The mobile phase consisted of 0.1% TFA in water and acetonitrile (65:35, v/v). The aqueous phase was adjusted to pH 3.1 using 0.1% (v/v) triethylamine. Before analysis, the mobile phase was filtered through a 0.45 µm cellulose acetate membrane filter and degassed by ultrasonication for 20 min. The flow rate was maintained at 1.0 ml/min, the column temperature at 25 ˚C, the injection volume was 50 µl, and detection was performed at 344 nm.

Calibration standards covering the concentration range of 0.1-50 µg/ml were prepared by serial dilution of the berberine stock solution with the mobile phase and analyzed in triplicate. The analytical method was validated according to the International Council for Harmonization (ICH Q2(R1)) guideline for linearity, precision, accuracy, specificity, limit of detection (LOD), limit of quantification (LOQ), and solution stability before use in quantitative analyses (28).

In vitro drug release study

The *in vitro* release of berberine from the optimized nanoemulgel, the corresponding nanoemulsion, and the conventional berberine gel was evaluated using vertical Franz diffusion cells (PermeGear Inc., Hellertown, PA, USA) with an effective diffusion area of 4.91 cm^2. A Spectra/Por® dialysis membrane (molecular weight cut-off (MWCO) 12,000–14,000 Da) was mounted between the donor and receptor compartments after appropriate hydration. The receptor compartment was filled with phosphate buffer (pH 5.5) and maintained at 32±0.5 ˚C throughout the experiment (29).

An accurately measured amount of each formulation (1 g) was placed in the donor compartment and evenly spread over the entire membrane surface. At predetermined time intervals (0.5, 1, 2, 3, 4, 5, 6, 7, and 24 h), 1 ml aliquots were withdrawn from the receptor compartment and immediately replaced with an equal volume (1 ml) of fresh phosphate buffer maintained at the same temperature to maintain sink conditions.

The collected samples were analyzed using the validated

Corrected Proof

HPLC method. The cumulative amount of berberine released was calculated after correcting for dilution from successive sampling and expressed as μg/cm². In addition, the cumulative percentage of drug released was calculated relative to the initial berberine amount in each formulation. The release profiles were expressed as both cumulative drug released per unit diffusion area and cumulative percentage drug released as a function of time.

To investigate the release mechanism, the release data were fitted to different mathematical models, including zero-order, first-order, Higuchi, Hixson-Crowell, and Korsmeyer-Peppas models (30). The most appropriate kinetic model was selected according to the coefficient of determination (R^2). Experiments were performed using three independent Franz diffusion cells for each formulation (n=3), and the results were expressed as mean±SD.

Ex vivo assessment of skin retention and receptor-compartment permeation

Because the developed nanoemulgel was intended for local topical rather than transdermal delivery, the *ex vivo* experiment was designed primarily to assess berberine retention within the skin. The receptor compartment was analyzed at the end of the 24-hr exposure period to determine the extent of drug passage across the skin; serial receptor sampling for characterization of transdermal permeation kinetics was not included in the experimental design.

The *ex vivo* skin distribution and retention study was performed using vertical Franz diffusion cells (PermeGear Inc., Hellertown, PA, USA) with an effective diffusion area of 4.91 cm² (29, 31). Fresh porcine ear skin, obtained from a local slaughterhouse, was used as the biological membrane. The skin was carefully prepared, visually inspected for physical damage, and mounted between the donor and receptor compartments with the stratum corneum facing the donor compartment.

The receptor compartment was filled with phosphate buffer (pH 7.4) and maintained at 37±0.5 ˚C throughout the experiment. An accurately measured amount of each formulation (0.5 g) was uniformly applied to the skin surface in the donor compartment.

After 24 hr, 1 ml of receptor medium was collected, and the berberine amount in the receptor compartment was quantified using the validated HPLC method. After the permeation experiment, the skin samples were removed from the diffusion cells, and residual formulation on the skin surface was gently removed with paper towels moistened with distilled water. The cleaned skin samples were cut into small pieces and transferred into extraction tubes containing 2 ml of the HPLC mobile phase. The samples were vortex-mixed, sonicated for 2 hr, and centrifuged at 5000 rpm for 20 min. The resulting supernatants were filtered through 0.45 μm membrane filters before HPLC analysis.

The amounts of berberine that permeated through the skin and those retained within the skin tissue after 24 hr were determined separately. Experiments were performed using three separate skin specimens mounted in three independent Franz diffusion cells for each formulation (n=3), and the results were expressed as mean±SD.

Stability evaluation of nanoemulgels

Accelerated stability tests

All prepared nanoemulgel formulations underwent accelerated stability testing using the same centrifugation and thermal stress procedures applied to the corresponding nanoemulsions. Following each test, the formulations were visually inspected for any signs of phase separation, creaming, cracking, or drug precipitation. Subsequently, droplet size, PDI, and zeta potential were determined using the same analytical methods employed for nanoemulgel characterization. Based on the accelerated stability test results, the formulation with the most favorable physicochemical stability was selected for further three-month storage stability evaluation.

Three-month storage stability study

The storage stability of the optimized nanoemulgel was evaluated over three months under three different storage conditions: refrigerated conditions (2-8 ˚C), 25±2 ˚C/60% relative humidity (RH), and 40±2 ˚C/75% RH (32).

At predetermined time intervals (0, 1, 2, and 3 months), the formulation was visually inspected for any changes in appearance, including phase separation, color change, or drug precipitation. In addition, droplet size, PDI, zeta potential, pH, electrical conductivity, and viscosity were determined using the same analytical methods employed for nanoemulgel characterization.

Furthermore, the berberine content was determined for samples stored at 2-8 ˚C and 25±2 ˚C/60% RH using the validated HPLC method. Briefly, 0.1 g of nanoemulgel was accurately weighed into a 10 ml volumetric flask and diluted to volume with methanol (33). The mixture was vortex-mixed for 10 min and sonicated for 30 min to ensure complete berberine extraction from the gel matrix (32). Subsequently, 2 ml of the extract was transferred into a microcentrifuge tube and centrifuged at 5000 rpm for 20 min. The resulting supernatant was filtered through a 0.45 μm membrane filter into HPLC vials before chromatographic analysis. The berberine concentration was quantified by HPLC, and the drug content was expressed as the percentage of the initial drug content remaining.

Measurements were performed using three independently prepared samples (n=3), and the results were expressed as mean±SD.

Cell culture

HaCaT cells were cultured in DMEM supplemented with 10% FBS and 1% penicillin-streptomycin. The cells were maintained in a humidified incubator at 37 ˚C under an atmosphere of 5% CO_2. Once the cells reached approximately 80% confluence, they were detached with 0.25% trypsin-EDTA and routinely subcultured for subsequent experiments.

Cell viability assay

The cytocompatibility of berberine, berberine-loaded nanoemulsion, berberine-loaded nanoemulgel, and placebo nanoemulgel was assessed using the 3-(4,5-Dimethylthiazol-2-yl)-2,5-diphenyltetrazolium Bromide (MTT) assay in accordance with International Organization for Standardization (ISO) 10993-5 guidelines with minor modifications (34, 35).

Briefly, HaCaT cells were harvested with 0.25% trypsin-EDTA, counted with a Thoma hemocytometer, and suspended in complete DMEM at 1×10^5 cells/ml. Subsequently, 100 μl of the cell suspension was seeded into

Corrected Proof

each well of a 96-well plate, corresponding to approximately 1×10^4 cells per well. The cells were allowed to adhere for 24 hr under standard culture conditions (37 ˚C and 5% CO_2).

After cell attachment, the culture medium was replaced with fresh medium containing serial concentrations of berberine, berberine-loaded nanoemulsion, berberine-loaded nanoemulgel, and placebo nanoemulgel, and the cells were incubated for an additional 24 hr. After treatment, 10 µl of MTT solution was added to each well, and the plates were incubated for 4 hr in the dark to allow intracellular formazan crystal formation. The supernatant was then carefully removed, and the crystals were dissolved in dimethyl sulfoxide. Absorbance was measured at 570 nm using a microplate reader. Cell viability was expressed as the percentage of viable cells relative to untreated control cells. All experiments were performed in triplicate.

In vitro scratch assay

The effects of berberine and the optimized berberine-loaded nanoemulgel on HaCaT scratch closure were evaluated using an *in vitro* scratch assay. The assay was performed according to a previously reported method with minor modifications (36).

HaCaT cells were cultured in complete DMEM supplemented with 10% FBS and 1% penicillin-streptomycin until they reached approximately 80% confluence. A linear scratch was then created across the cell monolayer using a sterile pipette tip to simulate a wound. Detached cells and cellular debris were carefully removed by gently rinsing the wells with serum-free DMEM.

The cells were subsequently treated with the highest non-cytotoxic concentrations of berberine and the optimized berberine-loaded nanoemulgel, as determined by the MTT assay. Untreated cells served as the negative control. Images of the scratch area were captured immediately after scratch formation (0 h) and again after 24 hr of incubation under standard culture conditions (37 ˚C, 5% CO_2).

Cell migration was assessed by comparing the wound area at 24 hr with that at 0 hr, and the extent of scratch closure was expressed as the percentage of the initial wound area. All experiments were performed in triplicate.

Statistical analysis

Statistical analyses were performed using Python (version 3.12.1) with NumPy (version 1.26.4), pandas (version 2.2.0), SciPy (version 1.12.0), Statsmodels (version 0.14.2), and Matplotlib (version 3.5.2). Quantitative data are presented as mean±SD, and a P-value<0.05 was considered statistically significant. No a priori power analysis was performed because the study was designed as an exploratory formulation-development investigation. Quantitative evaluations were generally performed in triplicate (n=3), with separate samples or experimental units used as applicable to each assay.

Prior to ANOVA, normality and homogeneity of variance were assessed using the Shapiro–Wilk and Levene's tests, respectively. No significant violations of these assumptions were detected for the physicochemical or scratch-assay datasets (P>0.05). For the cytocompatibility dataset, homogeneity of variance was met, whereas the two-way ANOVA residuals showed a departure from normality; therefore, the robustness of the factorial effects was additionally evaluated using heteroskedasticity-consistent HC3 covariance estimates.

The physicochemical characteristics of the freshly prepared nanoemulsions were analyzed using one-way ANOVA followed by Tukey's honestly significant difference (HSD) *post hoc* test. Cytocompatibility data were analyzed using two-way ANOVA with formulation and concentration as factors; following a significant interaction, Tukey's HSD multiple-comparisons test was used to compare formulations within each concentration. Scratch-closure percentages were analyzed using one-way ANOVA followed by Tukey's HSD *post hoc* test.

For pairwise comparisons performed using Tukey's HSD test, effect estimates are reported as mean differences with corresponding Tukey-adjusted simultaneous 95% confidence intervals (CIs) and multiplicity-adjusted P-values, where applicable.

Results

Development and physicochemical characterization of berberine-loaded nanoemulsions

Six berberine-loaded nanoemulsion formulations were prepared by varying the concentrations of berberine and QSS. Table 2 presents the physicochemical characteristics of the freshly prepared formulations and their responses to accelerated stability testing.

The mean droplet sizes of the freshly prepared nanoemulsions ranged from 76.10±1.71 to 135.73±3.39 nm, confirming the formation of nanosized dispersions. Significant differences in droplet size were detected among

Table 2. Physicochemical characteristics of freshly prepared berberine-loaded nanoemulsions

Formulation	Berberine (% w/w)	QSS (% w/w)	Droplet size (nm)	PDI	Zeta potential (mV)
NE1.1	0.5	5	117.53±1.15 ^{b}	0.225±0.006 ^{b}	−31.17±0.60 ^{b}
NE1.2	0.5	7	110.97±1.89 ^{b}	0.180±0.003 ^{c}	−30.30±0.87 ^{b}
NE1.3	0.5	10	77.18±3.46 ^{d}	0.244±0.018 ^{b}	−30.23±0.85 ^{b}
NE2.1	1.0	5	135.73±3.39 ^{a}	0.171±0.003 ^{c}	−23.33±1.63 ^{a}
NE2.2	1.0	7	91.60±3.76 ^{c}	0.230±0.011 ^{b}	−31.50±1.31 ^{b}
NE2.3	1.0	10	76.10±1.71 ^{d}	0.390±0.018 ^{a}	−28.63±0.81 ^{b}

Values are expressed as mean±SD (n=3). Different superscript letters (a-d) within the same column indicate statistically significant differences according to Tukey's HSD test (P<0.05). Effect estimates and corresponding Tukey-adjusted simultaneous 95% confidence intervals for all pairwise comparisons are provided in Supplementary Table S1
NE=nanoemulsion; QSS=Quillaja saponaria saponins; PDI=polydispersity index

Corrected Proof

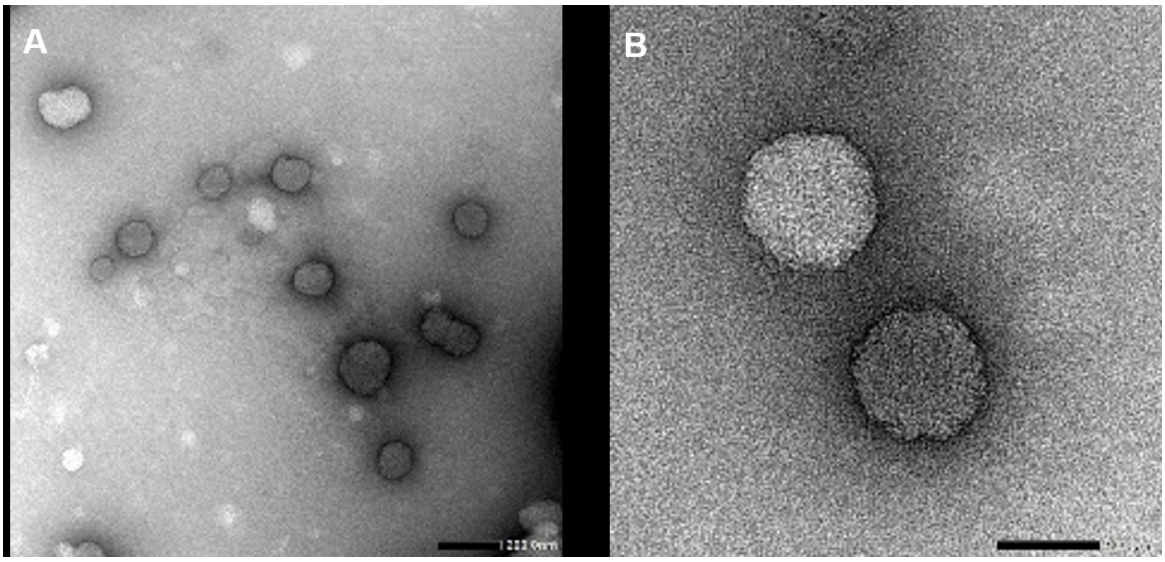


Figure 1. Transmission electron microscopy (TEM) images of the selected NE1.3 berberine-loaded nanoemulsion
(A) Representative TEM micrograph showing the overall morphology and distribution of the dispersed droplets (×15,000; scale bar=200 nm). (B) Higher-magnification TEM micrograph showing the morphology and boundaries of individual droplets (×50,000; scale bar = 100 nm). NE=nanoemulsion

the formulations [F(5,12)=226.305, *P*<0.0001]. At both berberine concentrations, increasing the QSS concentration from 5% to 10% was associated with a progressive reduction in droplet size. In the formulations containing 0.5% berberine, the mean droplet size decreased from 117.53±1.15 nm for NE1.1 to 77.18±3.46 nm for NE1.3. Similarly, among the formulations containing 1.0% berberine, the droplet size decreased from 135.73±3.39 nm for NE2.1 to 76.10±1.71 nm for NE2.3. Although the mean droplet sizes of NE1.3 and NE2.3 did not differ significantly (mean difference for NE1.3 minus NE2.3: 1.08 nm; 95% CI: -6.46 to 8.62 nm; adjusted *P*=0.996), NE1.3 exhibited a significantly lower PDI than NE2.3 (mean difference: −0.146; 95% CI: −0.178 to −0.114; adjusted *P*<0.001). Compared with NE1.2, NE1.3 exhibited a significantly smaller mean droplet size (mean difference: -33.79 nm; 95% CI: -41.33 to -26.25 nm; adjusted *P*<0.001).

Initial PDI values ranged from 0.171±0.003 to 0.390±0.018 and differed significantly among formulations [F(5,12)=137.994, *P*<0.0001]. All formulations except NE2.3 exhibited PDI values below 0.30. NE2.3 had a significantly higher PDI than all other formulations (*P*<0.0001), indicating a comparatively broader droplet size distribution despite its small mean droplet size.

All formulations exhibited negative zeta potentials, ranging from -23.33±1.63 to -31.50±1.31 mV. A significant difference was observed among the formulations [F(5,12)=24.220, *P*<0.0001]. NE2.1 exhibited the least negative zeta potential and differed significantly from all other formulations, whereas no significant differences were detected among the remaining nanoemulsions.

Morphological characterization by transmission electron microscopy (TEM)

TEM analysis of the selected NE1.3 nanoemulsion directly visualized the dispersed droplets (Figure 1). The micrographs revealed predominantly discrete, approximately spherical to slightly irregular droplets with clearly distinguishable boundaries. Although some droplets appeared in proximity or in small groups, the examined fields showed no extensive large-scale aggregation. Higher-magnification imaging further demonstrated the morphology and distinct boundaries of individual droplets.

Accelerated stability of berberine-loaded nanoemulsions

The formulations containing 0.5% berberine (NE1.1, NE1.2, and NE1.3) showed no visible phase separation, creaming, sedimentation, or drug precipitation after centrifugation or thermal stress testing. Although accelerated stress conditions caused statistically significant changes in droplet size, all three formulations retained nanoscale droplet sizes (Table 3).

For NE1.1, the mean droplet size decreased from 117.53±1.15 nm at T0 to 95.17±0.98 nm after centrifugation and 106.47±0.75 nm after thermal stress [F(2,6)=396.172,

Table 3. Physicochemical characteristics after accelerated stability testing

Formulation	Condition	Droplet size (nm)	PDI	Zeta potential (mV)
NE1.1	Initial, T0	117.53 ± 1.15^{x}	0.225 ± 0.006^{x}	−31.17 ± 0.60^{y}
	After centrifugation	95.17 ± 0.98^{z}	0.138 ± 0.002^{y}	−28.80 ± 2.09^{xy}
	After thermal stress	106.47 ± 0.75^{y}	0.229 ± 0.009^{x}	−26.07 ± 2.27^{x}
NE1.2	Initial, T0	110.97 ± 1.89^{y}	0.180 ± 0.003^{x}	−30.30 ± 0.87^{y}
	After centrifugation	101.52 ± 2.92^{z}	0.139 ± 0.024^{x}	−26.67 ± 1.86^{xy}
	After thermal stress	126.23 ± 2.53^{x}	0.176 ± 0.023^{x}	−25.23 ± 1.91^{x}
NE1.3	Initial, T0	77.18 ± 3.46^{y}	0.244 ± 0.018^{x}	−30.23 ± 0.85^{x}
	After centrifugation	83.26 ± 2.61^{y}	0.253 ± 0.007^{x}	−28.07 ± 1.66^{x}
	After thermal stress	95.03 ± 4.90^{x}	0.263 ± 0.018^{x}	−26.13 ± 3.10^{x}
NE2.1	After centrifugation	Phase separation	Not determined	Not determined
	After thermal stress	Phase separation	Not determined	Not determined
NE2.2	After centrifugation	Phase separation	Not determined	Not determined
	After thermal stress	Phase separation	Not determined	Not determined
NE2.3	After centrifugation	Phase separation	Not determined	Not determined
	After thermal stress	Phase separation	Not determined	Not determined

Values are expressed as mean±SD (n=3). Different superscript letters (x-z) within the same physicochemical parameter and within each formulation indicate statistically significant differences among the initial (T0), post-centrifugation, and post-thermal stress measurements (*P*<0.05, one-way ANOVA followed by Tukey's HSD *post hoc* test)
NE = nanoemulsion; PDI = polydispersity index; T0 = initial time point

Corrected Proof

P<0.0001]. Its PDI decreased significantly after centrifugation but returned to a value comparable to the initial measurement following thermal stress. After thermal stress, the zeta potential became significantly less negative than at T0, while the post-centrifugation value did not differ significantly from either condition.

For NE1.2, centrifugation reduced the droplet size to 101.52±2.92 nm, whereas thermal stress increased it to 126.23±2.53 nm [F(2,6)=75.695, *P*<0.0001]. Despite these changes, the PDI remained statistically unchanged among the three conditions. The zeta potential became less negative after thermal stress than it was initially.

NE1.3 showed no significant change in droplet size after centrifugation; however, thermal stress increased the size from 77.18±3.46 to 95.03±4.90 nm [F(2,6)=17.318, *P*=0.0032]. Neither PDI nor zeta potential changed significantly during the accelerated stability tests.

In contrast, all nanoemulsions containing 1.0% berberine (NE2.1, NE2.2, and NE2.3) underwent macroscopic phase separation during both centrifugation and thermal stress testing. Consequently, post-stress droplet size, PDI, and zeta potential measurements were not performed for these formulations, and they were excluded from subsequent nanoemulgel development.

Physicochemical characterization of berberine-loaded nanoemulgels

Six nanoemulgel formulations were obtained by incorporating the selected nanoemulsions into gels containing either 1% or 2% xanthan gum. Table 4 presents their initial physicochemical characteristics.

The mean droplet sizes of the freshly prepared nanoemulgels ranged from 100.79±11.48 to 238.03±8.22 nm and differed significantly among the formulations [F(5,12)=62.831, *P*<0.0001]. The nanoemulgels containing 2% xanthan gum generally exhibited larger droplet sizes than the corresponding formulations containing 1% xanthan gum. NEJ1.1 and NEJ1.2 with 1% xanthan gum had comparable droplet sizes, whereas NEJ1.1 with 2% xanthan gum had the highest mean droplet size. Among the 2% xanthan gum formulations, the droplet size decreased from NEJ1.1 to NEJ1.3.

The initial PDI values ranged from 0.223±0.020 to 0.364±0.007, with significant differences among the formulations [F(5,12)=83.593, *P*<0.0001]. NEJ1.1 and NEJ1.2 containing 1% xanthan gum, as well as NEJ1.1 containing 2% xanthan gum, exhibited significantly higher PDI values than the remaining formulations. In contrast, NEJ1.3 containing 1% xanthan gum and NEJ1.2 and NEJ1.3 containing 2% xanthan gum showed PDI values close to or below 0.23.

All nanoemulgels exhibited negative zeta potentials, ranging from -32.50±1.55 to -43.00±1.25 mV. Significant differences were detected among the formulations [F(5,12)=12.544, *P*=0.0002]. NEJ1.2 containing 1% xanthan gum showed a significantly less negative zeta potential than the other nanoemulgels, whereas no significant differences were observed among the remaining formulations.

Comparison of nanoemulsions and their corresponding nanoemulgels

Incorporating the nanoemulsions into xanthan gum gels produced formulation-dependent changes in physicochemical characteristics. For the NE1.1 and NE1.2 series, adding 1% xanthan gum did not significantly alter the initial droplet size compared with the corresponding parent nanoemulsions. However, increasing the xanthan gum concentration to 2% significantly increased droplet size in both series. In the NE1.3 series, both 1% and 2% xanthan gum nanoemulgels exhibited significantly larger droplet sizes than the parent nanoemulsion, with a further increase observed at the higher polymer concentration.

The PDI increased significantly following nanoemulgel formation in the NE1.1 series. In the NE1.2 series, both nanoemulgels also showed significantly higher PDI values than the parent nanoemulsion, although the increase was less pronounced for the formulation containing 2% xanthan gum. No significant differences in PDI were detected between NE1.3 and its corresponding nanoemulgels.

Nanoemulgel formation generally shifted the zeta potential toward more negative values. Both NEJ1.1 formulations and both NEJ1.3 formulations exhibited significantly more negative zeta potentials than their corresponding parent nanoemulsions. In the NE1.2 series, only the formulation containing 2% xanthan gum showed a significant shift.

Accelerated stability evaluation of berberine-loaded nanoemulgels

Table 5 summarizes the effects of centrifugation and thermal stress on the physicochemical characteristics of the nanoemulgels. All six formulations showed significant changes in droplet size after accelerated stress testing.

Corrected Proof

Table 4. Initial physicochemical characteristics of berberine-loaded nanoemulgels

Formulation	Xanthan gum (% w/w)	Droplet size (nm)	PDI	Zeta potential (mV)
NEJ1.1	1	100.79 ± 11.48^{d}	0.364 ± 0.007^{a}	−39.63 ± 0.81^{b}
NEJ1.2	1	107.24 ± 24.58^{d}	0.353 ± 0.007^{a}	−32.50 ± 1.55^{a}
NEJ1.3	1	142.97 ± 10.58^{c}	0.232 ± 0.016^{b}	−38.73 ± 2.85^{b}
NEJ1.1	2	238.03 ± 8.22^{a}	0.346 ± 0.015^{a}	−43.00 ± 1.25^{b}
NEJ1.2	2	221.57 ± 5.87^{ab}	0.223 ± 0.020^{b}	−40.10 ± 1.10^{b}
NEJ1.3	2	188.93 ± 5.13^{b}	0.224 ± 0.010^{b}	−40.37 ± 1.94^{b}

Values are expressed as mean±SD (n=3). Different superscript letters within the same column indicate statistically significant differences among the freshly prepared nanoemulgel formulations (*P*<0.05, one-way ANOVA followed by Tukey's HSD *post hoc* test)
NEJ=nanoemulgel; PDI = polydispersity index

Table 5. Effect of accelerated stability tests on the physicochemical characteristics of berberine-loaded nanoemulgels

Formulation	Xanthan gum (%)	Condition	Droplet size (nm)	PDI	Zeta potential (mV)
NEJ1.1	1	Initial, T0	100.79 ± 11.48^{y}	0.364 ± 0.007^{y}	−39.63 ± 0.81^{y}
		After centrifugation	182.20 ± 4.64^{x}	0.245 ± 0.015^{z}	−35.03 ± 1.29^{x}
		After thermal stress	73.05 ± 0.95^{z}	0.506 ± 0.009^{x}	−35.10 ± 0.95^{x}
NEJ1.2	1	Initial, T0	107.24 ± 24.58^{y}	0.353 ± 0.007^{y}	−32.50 ± 1.55^{x}
		After centrifugation	180.70 ± 1.95^{x}	0.435 ± 0.022^{x}	−32.97 ± 1.10^{x}
		After thermal stress	71.88 ± 2.88^{y}	0.466 ± 0.010^{x}	−34.60 ± 0.62^{x}
NEJ1.3	1	Initial, T0	142.97 ± 10.58^{x}	0.232 ± 0.016^{z}	−38.73 ± 2.85^{y}
		After centrifugation	82.03 ± 0.91^{y}	0.491 ± 0.005^{x}	−29.37 ± 0.87^{x}
		After thermal stress	64.86 ± 4.33^{z}	0.401 ± 0.003^{y}	−30.13 ± 1.63^{x}
NEJ1.1	2	Initial, T0	238.03 ± 8.22^{y}	0.346 ± 0.015^{y}	−43.00 ± 1.25^{y}
		After centrifugation	270.37 ± 0.97^{x}	0.286 ± 0.008^{y}	−39.10 ± 0.85^{x}
		After thermal stress	78.60 ± 5.67^{z}	0.775 ± 0.064^{x}	−40.80 ± 0.50^{xy}
NEJ1.2	2	Initial, T0	221.57 ± 5.87^{y}	0.223 ± 0.020^{z}	−40.10 ± 1.10^{x}
		After centrifugation	262.27 ± 12.87^{x}	0.271 ± 0.008^{y}	−38.80 ± 2.03^{x}
		After thermal stress	81.77 ± 7.79^{z}	0.537 ± 0.012^{x}	−36.37 ± 2.08^{x}
NEJ1.3	2	Initial, T0	188.93 ± 5.13^{x}	0.224 ± 0.010^{y}	−40.37 ± 1.94^{x}
		After centrifugation	159.73 ± 5.36^{y}	0.224 ± 0.017^{y}	−39.23 ± 1.10^{x}
		After thermal stress	129.77 ± 1.06^{z}	0.323 ± 0.013^{x}	−37.87 ± 2.41^{x}

Values are expressed as mean±SD (n=3). Different superscript letters within the same physicochemical parameter and within each formulation indicate statistically significant differences among the initial (T0), post-centrifugation, and post-thermal stress measurements (P<0.05, one-way ANOVA followed by Tukey's HSD *post hoc* test)
NEJ = nanoemulgel; PDI = polydispersity index; T0 = initial time point

For NEJ1.1 containing 1% xanthan gum, centrifugation increased the droplet size from 100.79±11.48 to 182.20±4.64 nm, whereas thermal stress reduced it to 73.05±0.95 nm [$F(2,6)=187.948$, P<0.0001]. The PDI decreased after centrifugation but increased to 0.506±0.009 following thermal stress. The zeta potential became significantly less negative after both stress procedures.

NEJ1.2 containing 1% xanthan gum showed an increase in droplet size after centrifugation, while the post-thermal stress value did not differ significantly from the initial measurement. Both centrifugation and thermal stress produced significantly higher PDI values than T0. Zeta potential did not change significantly.

For NEJ1.3 containing 1% xanthan gum, both centrifugation and thermal stress significantly reduced the measured droplet size. The PDI increased from 0.232±0.016 at T0 to 0.491±0.005 after centrifugation and 0.401±0.003 after thermal stress. Its zeta potential also became significantly less negative following both stress tests.

Among the formulations containing 2% xanthan gum, NEJ1.1 and NEJ1.2 exhibited increased droplet sizes after centrifugation, followed by substantially lower values after thermal stress. Their post-thermal stress PDI values increased to 0.775±0.064 and 0.537±0.012, respectively. NEJ1.3 containing 2% xanthan gum showed progressive reductions in droplet size following centrifugation and thermal stress. Its PDI remained unchanged after centrifugation but increased significantly after thermal stress. No statistically significant changes in zeta potential were detected for NEJ1.2 or NEJ1.3 containing 2% xanthan gum. Importantly, the lower mean droplet-size values observed after thermal stress were generally accompanied by increased PDI values, indicating a broader and more heterogeneous particle-size distribution rather than a uniform reduction in droplet dimensions.

Rheological characterization of the selected nanoemulgel

Figure 2 presents the rheological behavior of the selected nanoemulgel (NEJ1.3 containing 2% xanthan gum). The formulation exhibited a progressive decrease in viscosity with increasing shear rate, indicating a typical non-Newtonian shear-thinning flow behavior. The mean viscosity decreased from 260.62±4.16 cP at 75 s^{-1} to 50.30±1.76 cP at 750 s^{-1} (Figure 2).

The experimental data showed excellent agreement with the Power Law model, yielding a consistency index (K) of 5.513 Pa·s^n, a flow behavior index (n) of 0.289, and a coefficient of determination (R^2) of 0.9979. The n value, substantially lower than unity, confirmed the pronounced pseudoplastic behavior of the selected nanoemulgel.

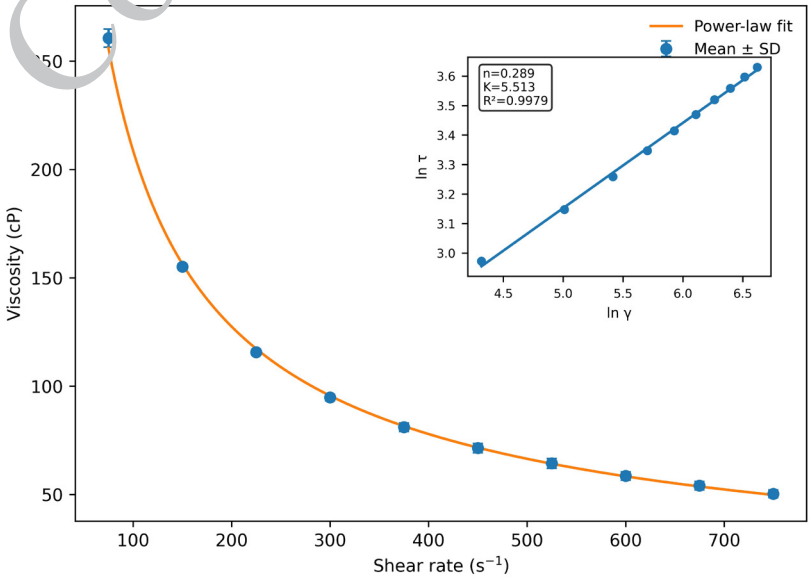


Figure 2. Rheological behavior of the selected berberine-loaded nanoemulgel (NEJ1.3 containing 2% xanthan gum)
Viscosity is expressed as mean±standard deviation (n=3) as a function of shear rate. The inset shows the logarithmic transformation of the Power Law model (natural logarithm of shear stress versus natural logarithm of shear rate) together with the fitted regression line
NEJ = nanoemulgel

Corrected Proof

Mechanical properties and spreadability of the selected nanoemulgel

The mechanical and spreadability properties of the optimized berberine-loaded nanoemulgel were compared with those of the conventional berberine gel, and the results are presented in Table 6**.** The nanoemulgel exhibited greater hardness than the conventional gel (11.66±0.13 vs. 7.59±0.10 g). Likewise, the magnitude of adhesiveness was higher for the nanoemulgel, indicating stronger adhesion to the probe surface during withdrawal. The conventional gel showed slightly higher cohesiveness (0.880±0.027) and resilience (0.271±0.017) than the nanoemulgel (0.839±0.042 and 0.127±0.005, respectively), whereas both formulations had comparable springiness values close to unity.

The spreadability test further demonstrated marked differences between the formulations. The nanoemulgel exhibited higher firmness (47.61±0.32 g) and required substantially greater work of shear for spreading (29.88±1.95 g·s) than the conventional gel (26.21±0.62 g and 7.27±0.01 g·s, respectively), reflecting its greater mechanical strength and resistance to deformation during spreading.

Table 6. Mechanical properties and spreadability characteristics of the conventional gel and the optimized berberine-loaded nanoemulgel

Parameter	Conventional gel	optimized nanoemulgel
Hardness (g)	7.59 ± 0.10	11.66 ± 0.13
Adhesiveness (g·s)	−2.88 ± 1.25	−6.58 ± 0.13
Cohesiveness	0.880 ± 0.027	0.839 ± 0.042
Springiness	0.971 ± 0.042	1.000 ± 0.000
Resilience	0.271 ± 0.017	0.127 ± 0.005
Firmness (g)	26.21 ± 0.62	47.61 ± 0.32
Work of shear (g·s)	7.27 ± 0.01	29.88 ± 1.95

Values are expressed as mean±standard deviation (n = 3)

Validation of the HPLC method

The developed RP-HPLC method provided a well-defined berberine peak without interference from formulation excipients, receptor medium components, or skin extract, confirming the specificity of the analytical procedure.

Excellent linearity was obtained over the concentration range of 0.1-50 µg/ml, with the calibration curve described by the regression equation y=195489x−15111 and a correlation coefficient (R^2) of 0.9999. The analytical method also demonstrated satisfactory precision, with intra-day and inter-day relative standard deviation (RSD) values below 1.5% and 0.3%, respectively. Recovery values ranged from 98.88% to 101.26%, indicating good analytical accuracy. Furthermore, the calculated LOD and LOQ values were 0.00263 ng/ml and 0.00798 ng/ml, respectively, demonstrating high analytical sensitivity. Solution stability studies confirmed that berberine remained stable in the analytical solution for at least 48 hr, with negligible variation in the measured concentrations. These results demonstrated that the validated RP-HPLC method was suitable for the quantitative determination of berberine throughout the study.

In vitro drug release

Figure 3 presents the *in vitro* release profiles of berberine from the optimized nanoemulgel, nanoemulsion, and conventional gel. All formulations showed a time-dependent increase in cumulative drug release over 24 hr.

The conventional gel exhibited the fastest release profile, reaching 591.00±20.21 µg/cm², corresponding to 87.93±3.01%, at 24 hr. The nanoemulsion showed an intermediate release profile, with a cumulative release of 458.29±17.38 µg/cm² and 68.19±2.59% at 24 hr. The optimized nanoemulgel displayed the slowest release profile, reaching 424.87±15.11 µg/cm², equivalent to 63.22±2.25%, after 24 hr.

Drug release kinetics

To further elucidate the release mechanism of berberine

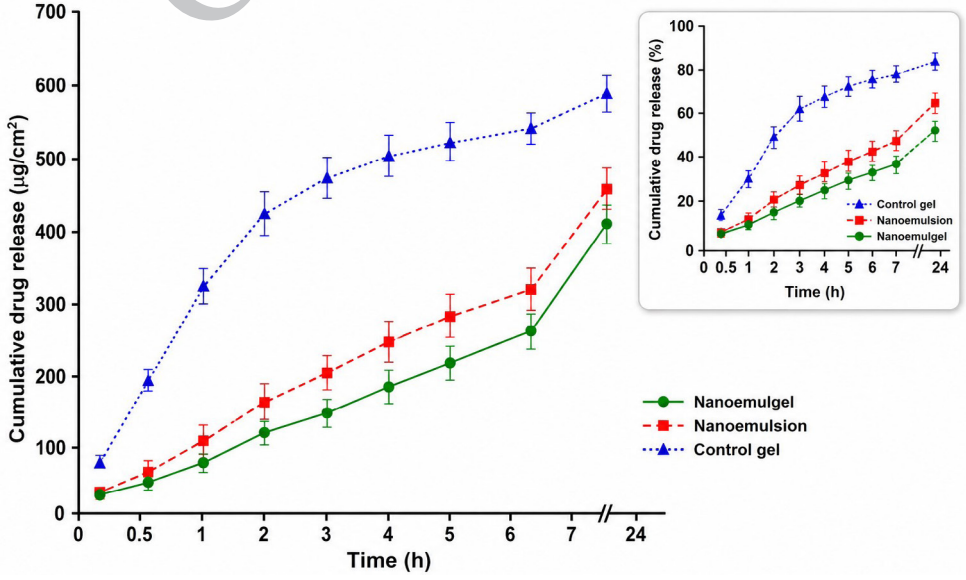


Figure 3. *In vitro* cumulative release profiles of berberine from the optimized nanoemulgel, nanoemulsion, and conventional gel
The main graph shows the cumulative amount of drug released per unit area (µg/cm²), whereas the inset illustrates cumulative drug release expressed as the percentage of the initial drug content. Data are expressed as mean±standard deviation (n=3)

Corrected Proof

from the investigated formulations, the release data were fitted to zero-order, first-order, Higuchi, and Korsmeyer–Peppas kinetic models. Table 7 summarizes the calculated kinetic parameters, and Figure 4 presents the linearized Higuchi and Korsmeyer–Peppas plots.

Among the evaluated kinetic models, the Korsmeyer–Peppas model exhibited the highest coefficients of determination (R^2) for all formulations, indicating the best agreement with the experimental release data. The optimized nanoemulgel and nanoemulsion showed excellent fits (R^2=0.9995 and 0.9984, respectively), while the conventional gel also showed satisfactory agreement (R^2=0.9705).

The release exponent (n) obtained from the Korsmeyer–Peppas model was 0.759 for the nanoemulgel, 0.824 for the nanoemulsion, and 1.128 for the conventional gel.

Among the remaining models, the Higuchi model provided the second-highest R^2 values for the nanoemulgel (R^2=0.972) and nanoemulsion (R^2=0.938). Comparatively lower R^2 values were obtained with the zero-order and first-order models.

Table 7. Drug release kinetic parameters of berberine formulations

Kinetic model	Parameter	Nanoemulgel	Nanoemulsion	Conventional gel
Zero-order	k_0	15.37	16.30	15.78
	R^2	0.847	0.776	0.410
First-order	k_1 (h^{-1})	0.0388	0.0443	0.0725
	R^2	0.940	0.902	0.641
Higuchi	kH	96.09	104.64	116.49
	R^2	0.972	0.938	0.655
Korsmeyer–Peppas[1]	kKP	0.0908	0.0988	0.2382
	n	0.759	0.824	1.128
	R^2	0.9995	0.9984	0.9705

R^2=coefficient of determination; k_0=zero-order release constant; k_1=first-order release constant; kH=Higuchi release constant; kKP=Korsmeyer–Peppas release constant

Ex vivo skin permeation and deposition

Figure 5 presents the *ex vivo* skin permeation and deposition results after 24 hr. The nanoemulsion showed the

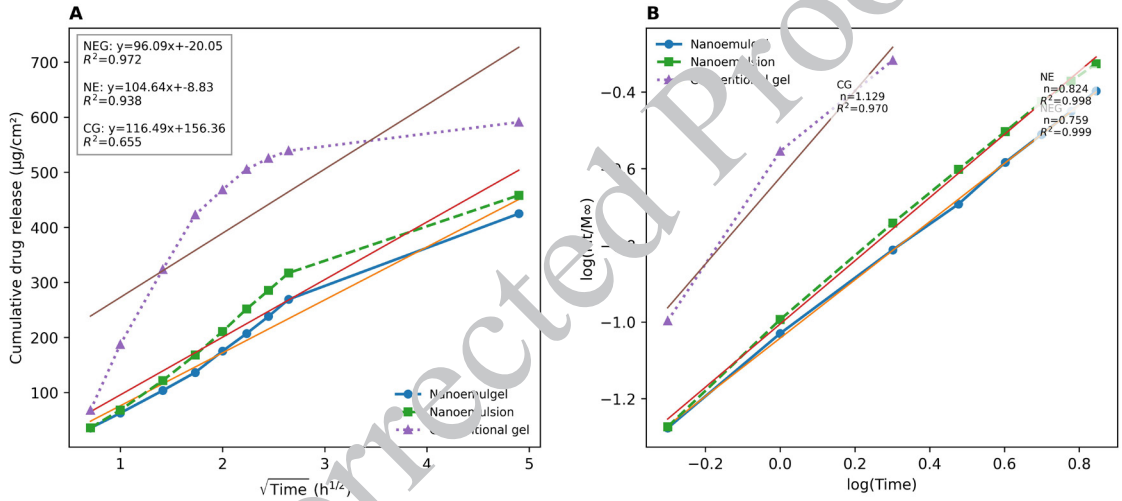


Figure 4. Linearized release kinetic models of berberine formulations
(A) Higuchi plots showing the relationship between cumulative drug release and the square root of time. (B) Korsmeyer–Peppas plots used to determine the release exponent (n) and characterize the release mechanism. The Korsmeyer–Peppas model was fitted using the initial release stage corresponding to cumulative drug release below approximately 60%

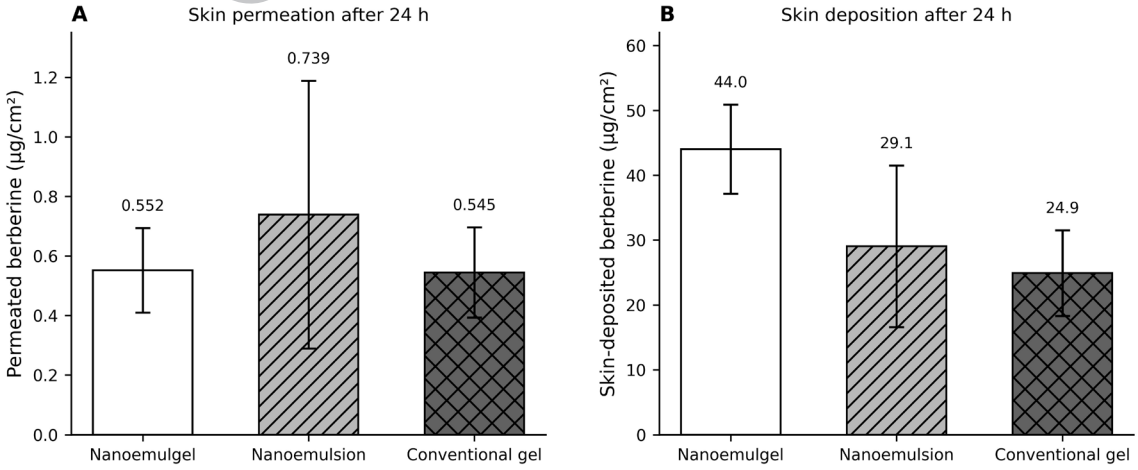


Figure 5. *Ex vivo* permeation and skin deposition of berberine from the nanoemulgel, nanoemulsion, and conventional gel after 24 hr
(A) Amount of berberine permeated through the skin into the receptor compartment. (B) Amount of berberine retained within the skin. Data are expressed as mean±standard deviation (n=3)

Corrected Proof

highest mean amount of berberine permeated through the skin, reaching 0.739±0.450 µg/cm². The amounts permeated from the nanoemulgel and conventional gel were lower and closely comparable, at 0.552±0.142 µg/cm² and 0.545±0.151 µg/cm², respectively.

In contrast, the nanoemulgel showed the highest skin deposition, with 44.014±6.865 µg/cm² of berberine retained in the skin. The corresponding deposition values for the nanoemulsion and conventional gel were 29.056±12.446 µg/cm² and 24.921±6.608 µg/cm², respectively. The nanoemulgel showed the highest mean skin deposition value, whereas the nanoemulsion showed the highest mean amount of berberine that permeated into the receptor compartment after 24 hr.

Three-month physicochemical stability of the optimized nanoemulgel

Figure 6 presents the three-month changes in mean droplet size, PDI, and zeta potential of the optimized nanoemulgel under refrigerated, room-temperature, and accelerated storage conditions.

The initial mean droplet size was 174.45±17.32 nm. After one month, the droplet size decreased to 134.85±2.33 nm at 2-8 ˚C and 140.00±0.42 nm at 25±2 ˚C/60% RH, whereas it was 166.50±2.55 nm under accelerated storage conditions. At the second month, the corresponding droplet sizes were 138.90±1.70 nm, 142.35±0.92 nm, and 178.10±8.34 nm, respectively. At the end of the third month, the formulation maintained mean droplet sizes of 137.60±5.94 nm at 2-8 ˚C, 143.40±2.12 nm at 25±2 ˚C/60% RH, and 175.80±0.57 nm at 40±2 ˚C/75% RH. Overall, the droplets remained within the nanoscale range throughout the storage period under all investigated conditions.

The initial PDI was 0.258±0.047. During refrigerated storage, the PDI remained between 0.23[illegible] and 0.244 over the three months. Similarly, the PDI values at 25±2 ˚C/60% RH ranged from 0.247 to 0.253. Under accelerated storage conditions, PDI decreased gradually from 0.232±0.003 in the first month to 0.218±0.008 in the third month. All PDI values remained below 0.30 throughout the three-month storage period under all investigated conditions.

The initial zeta potential was -35.95±0.07 mV. During the first two months, the formulation maintained strongly negative zeta potential values under all storage conditions. At the second month, the values were -33.40±2.40 mV, -38.70±1.84 mV, and -32.50±1.56 mV at 2-8 ˚C, 25±2 ˚C/60% RH, and 40±2 ˚C/75% RH, respectively. However, by the third month, the magnitude of the zeta potential decreased to -25.15±0.21 mV, -21.85±0.21 mV, and -21.70±1.70 mV, respectively. Despite this shift toward less negative values, the formulation retained a negative surface charge under all storage conditions.

Taken together, the optimized nanoemulgel maintained nanoscale droplet dimensions and PDI values below 0.30 throughout the three-month study. The most pronounced change occurred in zeta potential in the third month, while droplet size and distribution remained comparatively stable.

pH and conductivity stability

Figure 7 presents changes in pH and electrical conductivity of the optimized nanoemulgel during three months of storage under refrigerated, room-temperature, and accelerated conditions.

The initial pH of the formulation was 4.42±0.01. During storage, pH gradually decreased under all storage conditions. After three months, the pH values reached 4.29±0.0[illegible], 4.[illegible]1±0.02, and 4.16±0.02 at 2-8 ˚C, 25±2 ˚C/60% RH, and 40±2 ˚C/75% RH, respectively.

The initial electrical conductivity of the nanoemulgel was 107[illegible]±2.83 µS/cm. Throughout the storage period, conductivity values remained relatively constant under all storage conditions, ranging from 1073 to 1093 µS/cm. At the end of the third month, conductivity values were 1080.5±0.71 µS/cm, 1074±4.24 µS/cm, and 1091±2.83 µS/cm under refrigerated, room-temperature, and accelerated storage conditions, respectively. Overall, conductivity values varied within a relatively narrow range (1073-1093 µS/cm) throughout the three-month storage period.

Rheological stability during storage

Figure 8 presents the rheological stability of the optimized berberine-loaded nanoemulgel over three months under refrigerated (2-8 ˚C), room-temperature (25±2 ˚C/60% RH), and accelerated (40±2 ˚C/75% RH) conditions. The viscosity profiles at all storage conditions showed a progressive decrease with increasing shear rate, indicating that the

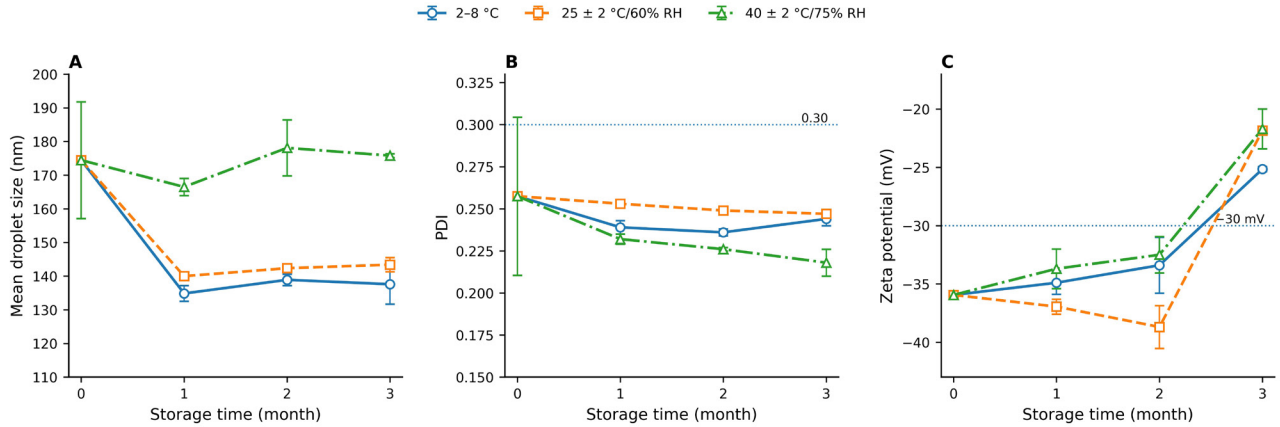


Figure 6. Three-month physicochemical stability of the optimized berberine-loaded nanoemulgel under refrigerated conditions (2-8 ˚C), room-temperature conditions (25±2 ˚C/60% relative humidity), and accelerated conditions (40±2 ˚C/75% relative humidity)
(A) Mean droplet size, (B) polydispersity index, and (C) zeta potential as a function of storage time. Data are expressed as mean±standard deviation (n=3). The dotted reference lines indicate a polydispersity index value of 0.30 and a zeta potential of -30 mV

Corrected Proof

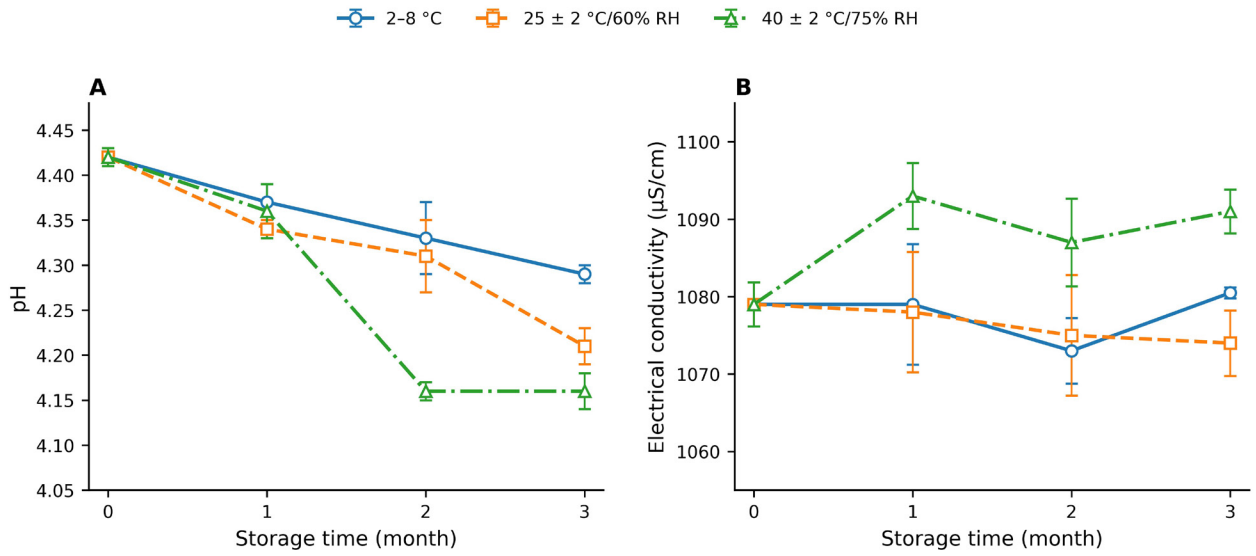


Figure 7. Changes in the pH and electrical conductivity of the optimized berberine-loaded nanoemulgel during three months of storage under refrigerated conditions (2-8 ˚C), room-temperature conditions (25±2 ˚C/60% relative humidity), and accelerated conditions (40±2 ˚C/75% relative humidity)
(A) pH and (B) electrical conductivity as a function of storage time. Data are expressed as mean±standard deviation (n=3)

formulation maintained its characteristic shear-thinning behavior throughout the storage period.

Under refrigerated storage, the viscosity profiles remained highly comparable to those obtained on Day 0. At the lowest shear rate (75 s^{-1}), the viscosity changed from 260.62±4.16 cP on Day 0 to 261.10±3.91 cP, 264.71±1.47 cP, and 278.04±1.85 cP after one, two, and three months, respectively. At the highest shear rate (750 s^{-1}), the corresponding viscosities were 50.30±1.76 cP, 47.41±1.48 cP, 47.34±1.02 cP, and 55.62±0.51 cP, demonstrating only minor variations during storage.

Similarly, formulations stored at 25±2 ˚C/60% RH retained rheological profiles closely resembling those measured initially. The viscosity at 75 s^{-1} remained essentially unchanged during the first two months (260.23±4.38 cP and 261.12±1.91 cP) and was 264.79±0.90 cP after three months. At 750 s^{-1}, viscosity values ranged from 51.24±3.08 cP to 55.36±0.43 cP, remaining close to the initial measurement.

Viscosity decreased more markedly under accelerated storage conditions. At 75 s^{-1}, the viscosity gradually decreased from 260.62±4.16 cP initially to 253.98±2.37 cP, 229.78±2.64 cP, and 220.26±0.20 cP after one, two, and three months, respectively. Similar decreases were observed across the entire shear-rate range. Despite the reduction in absolute viscosity values under accelerated storage conditions, viscosity continued to decrease with increasing shear rate at all evaluated time points.

Overall, the optimized nanoemulgel maintained its non-Newtonian, shear-thinning rheological behavior throughout the three-month storage period across all investigated conditions, although accelerated storage led to a moderate decrease in viscosity compared with refrigerated and room-temperature storage.

Drug content stability

The drug content stability of the optimized berberine-loaded nanoemulgel was evaluated over three months of storage at 4 ˚C and 25 ˚C. To assess changes in drug

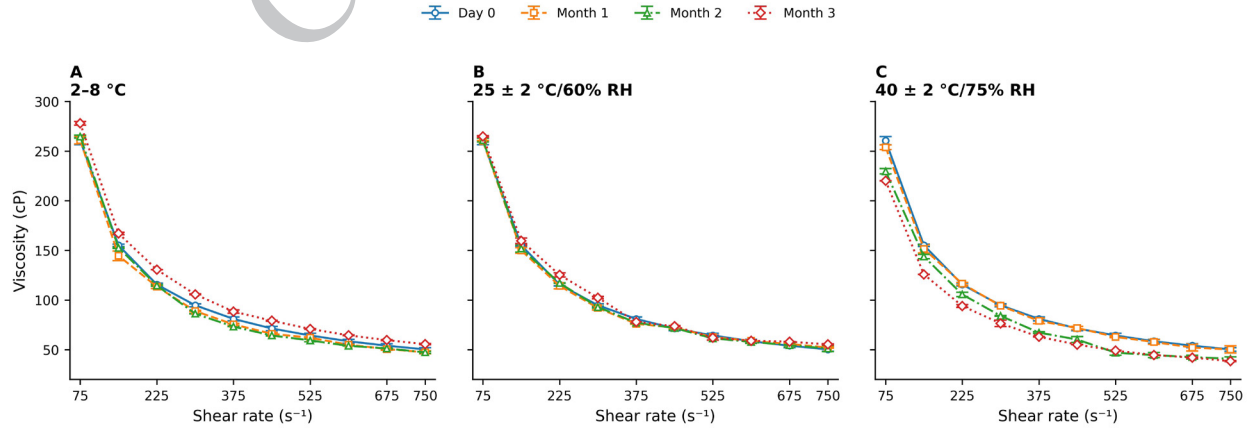


Figure 8. Rheological stability of the optimized berberine-loaded nanoemulgel during three months of storage under refrigerated conditions (2-8 ˚C), room-temperature conditions (25±2 ˚C/60% relative humidity), and accelerated conditions (40±2 ˚C/75% relative humidity)
Viscosity profiles obtained on Day 0 and after one, two, and three months of storage are shown for (A) 2-8 ˚C, (B) 25±2 ˚C/60% relative humidity, and (C) 40±2 ˚C/75% relative humidity. Data are expressed as mean±standard deviation (n=3)

Corrected Proof

content independent of the initial assay value, we defined the Day 0 drug content as 100% and expressed subsequent measurements as relative drug retention. At 4 ˚C, drug retention remained close to the initial value throughout the study, with values of 101.39±1.06%, 100.58±0.40%, and 99.73±0.10% after 1, 2, and 3 months, respectively. At 25 ˚C, drug retention was 99.60±1.59% after one month, then decreased to 85.96±5.76% and 86.14±1.58% after two and three months, respectively.

Cytocompatibility

The cytocompatibility of free berberine and the berberine-loaded formulations was evaluated in HaCaT cells after 24 hr of exposure using the MTT assay. Figure 9 presents the cell viability profiles. Two-way ANOVA demonstrated significant effects of formulation and concentration, as well as a significant formulation×concentration interaction (P<0.0001 for all factors). Therefore, Tukey's multiple-comparisons test was performed to compare the formulations at each concentration.

Cell viability generally decreased with increasing concentration, although the magnitude of this reduction differed among the formulations. At concentrations ranging from 0.78125 to 6.25 mg/ml, the mean cell viability remained above 80% in all groups.

At 12.5 mg/ml, the nanoemulgel exhibited the highest cell viability (82.43±0.35%), followed by the nanoemulsion (81.01±0.31%), free berberine (76.48±0.21%), and the conventional gel (70.13±0.82%). Post-hoc analysis showed that the nanoemulgel had significantly higher cell viability than the nanoemulsion (mean difference: 1.42 percentage points; 95% CI: 0.16-2.68; adjusted P=0.028[illegible]; [illegible] berberine (mean difference: 5.94 percentage points; 95% CI: 4.69-7.20; adjusted P<0.001), and the conventional gel (mean difference: 12.30 percentage points; 95% CI: 11.04-13.56; adjusted P<0.001). The nanoemulsion also showed significantly higher viability than free berberine (mean difference: 4.53 percentage points; 95% CI: 3.27-5.78; adjusted P<0.001) and the conventional gel (mean difference: 10.88 percentage points; 95% CI: 9.62-12.14; adjusted P<0.001). At 25 mg/ml, the nanoemulsion (77.05±0.86%), nanoemulgel (76.00±1.38%), and free berberine (74.96±0.62%) exhibited comparable cell viability, with the corresponding 95% CIs for the pairwise mean differences including zero. In contrast, the conventional gel (64.70±2.17%) showed significantly lower viability than free berberine (mean difference: -10.26 percentage points; 95% CI: -13.90 to -6.63; adjusted P=0.0001), the nanoemulsion (mean difference: −12.35 percentage points; 95% CI: -15.98 to -8.71; adjusted P<0.001), and the nanoemulgel (mean difference: -11.31 percentage points; 95% CI: -14.94 to -7.67; adjusted P<0.001). At the highest concentration (50 mg/ml), free berberine (68.64±1.05%), the nanoemulsion (68.16±0.34%), and the nanoemulgel (69.22±1.96%) produced statistically comparable cell viability values, with the corresponding 95% CIs for the pairwise mean differences including zero. In contrast, the conventional gel (60.07±4.91%) showed significantly lower viability than free berberine (mean difference: -8.57 percentage points; 95% CI: -15.64 to -1.51; adjusted P=0.0194), the nanoemulsion (mean difference: -8.10 percentage points; 95% CI: -15.16 to -1.05; adjusted P=0.0260), and the nanoemulgel (mean difference: -9.15 percentage points; 95% CI: -16.22 to -2.09; adjusted P=0.0136). Overall, mean cell viability remained [illegible]% for all tested formulations up to 12.5 mg/ml. At this concentration, the nanoemulgel showed the highest mean cell viability (82.43±0.35%). Supplementary Table S2 provides the complete set of pairwise comparisons across all tested concentrations, including mean differences, Tukey-adjusted simultaneous 95% confidence intervals, and adjusted P-values.

Corrected Proof

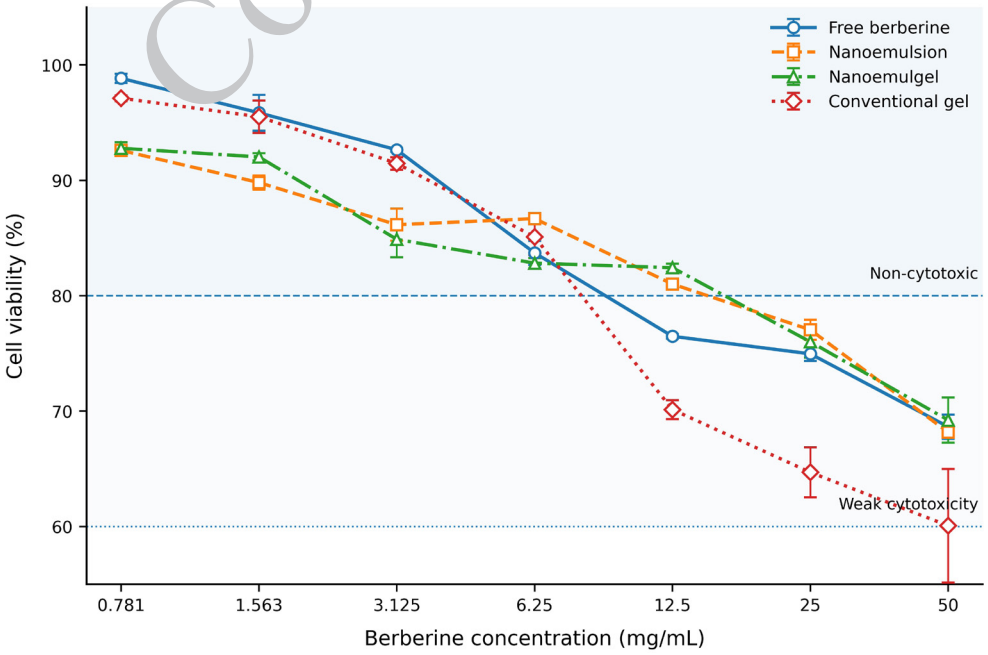


Figure 9. Cytocompatibility of free berberine, berberine-loaded nanoemulsion, berberine-loaded nanoemulgel, and conventional berberine gel in HaCaT keratinocytes after 24 hr of exposure
Cell viability was determined using the 3-(4,5-dimethylthiazol-2-yl)-2,5-diphenyltetrazolium bromide assay. Data are presented as mean±standard deviation (n=3). The horizontal dashed line represents 70% cell viability

In vitro scratch closure

The effects of free berberine and the nanoemulgel on HaCaT cell migration were investigated using the scratch assay. Figure 10 presents representative microscopic images from 0 and 24 hr, along with quantitative scratch-closure results.

Only limited spontaneous scratch closure was observed in the negative control group after 24 hr. Free berberine reduced the remaining scratch area, whereas the nanoemulgel group showed a greater reduction. The calculated scratch-closure values were 2.33±3.08%, 25.56±4.29%, and 76.33±3.43% for the negative control, free berberine, and nanoemulgel groups, respectively.

One-way ANOVA followed by Tukey's HSD multiple-comparison test showed significant differences among all groups. The berberine-loaded nanoemulgel produced significantly greater scratch closure than free berberine (mean difference: 50.77 percentage points; 95% CI: 41.66-59.88; adjusted $P<0.001$) and the negative control (mean difference: 74.00 percentage points; 95% CI: 64.88–83.11; adjusted $P<0.001$). Free berberine also produced significantly greater scratch closure than the negative control (mean difference: 23.23 percentage points; 95% CI: 14.12–32.34; adjusted $P=0.0006$). These findings demonstrate greater *in vitro* scratch closure with the berberine-loaded nanoemulgel than with free berberine under the experimental conditions used. However, because the scratch assay did not include a placebo nanoemulgel, the specific contribution of berberine cannot be distinguished from potential effects of the formulation excipients.

Discussion

Development and physicochemical characteristics of berberine-loaded nanoemulsions

Effect of Quillaja Saponin Concentration on Droplet Size, PDI and Zeta Potential

The freshly prepared berberine-loaded nanoemulsions exhibited mean droplet sizes ranging from 76.10 to 135.73 nm, confirming the successful production of nanoscale oil-in-water dispersions by probe ultrasonication. These droplet sizes are within the nanoscale range reported for topical nanoformulations. Nanosized droplets provide a large interfacial area and close contact with the skin surface, characteristics that may support topical drug delivery (17, 37).

The obtained droplet sizes also compare favorably with those reported for numerous topical nanoformulations developed for wound healing. Ahmad *et al.* prepared an ultrasonically produced curcumin nanoemulsion with a mean droplet size of approximately 94 nm (38). In contrast, Algahtani *et al.* reported a curcumin nanoemulsion with a droplet size of 56.25 nm before incorporating it into a Carbopol nanoemulgel (17). Similarly, Panda *et al.* developed berberine-loaded lecithin-chitosan nanoparticles with an average particle size of 168.4 nm (5). In comparison, Nguyen *et al.* reported berberine-loaded NLCs with a particle size of approximately 82 nm (39). More recently, Bahloul *et al.* obtained droplet sizes around 56 nm for Opuntia seed oil nanoemulgels (40), whereas Rehman *et al.* reported droplet sizes of approximately 139 nm for eucalyptol-loaded nanoemulgels (41). Collectively, these studies indicate that the droplet sizes obtained in the present study are within the nanoscale range commonly reported for topical nanocarrier systems. However, droplet size alone does not determine dermal delivery performance or biological efficacy, which also depend on formulation composition, interfacial properties, release behavior, skin interactions, and biological factors (5, 39, 40).

A clear concentration-dependent reduction in droplet size was observed as the QSS concentration increased from 5% to 10%. In formulations containing 0.5% berberine, the mean droplet diameter decreased from 117.53 nm to 77.18 nm, whereas in the 1.0% berberine formulations, the corresponding reduction was even more pronounced, decreasing from 135.73 nm to 76.10 nm. These findings clearly show that increasing the QSS concentration substantially improved emulsification efficiency under the selected ultrasonication conditions. The observed behavior can be explained by the increased availability of surfactant molecules for rapid adsorption onto the newly generated oil-water interface immediately after droplet disruption. Rapid interfacial coverage lowers interfacial free energy, suppresses recoalescence of freshly formed droplets, and ultimately produces smaller, more stable nanoemulsion droplets (17).

QSS's superior emulsification efficiency stems from its unique molecular architecture. Unlike conventional low-molecular-weight synthetic surfactants, QSS is an

Corrected Proof

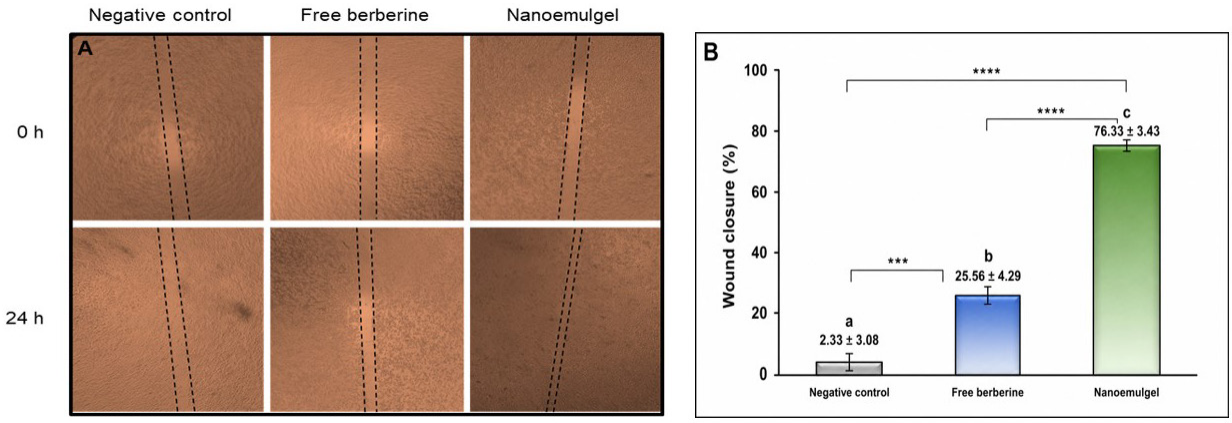


Figure 10. Effects of free berberine and berberine-loaded nanoemulgel on HaCaT keratinocyte scratch closure
(A) Representative microscopic images of the scratch area in the negative control, free berberine, and nanoemulgel groups at 0 and 24 hr. (B) Quantitative scratch closure after 24 hr. Data are presented as mean±standard deviation (n=3). Different letters indicate statistically significant differences between groups according to one-way analysis of variance followed by Tukey's honestly significant difference test ($P<0.05$)

amphiphilic biosurfactant consisting of a hydrophobic triterpenoid aglycone linked to hydrophilic oligosaccharide chains containing glucuronic acid residues. This structure enables rapid adsorption at the oil-water interface while simultaneously providing both electrostatic and steric stabilization. The bulky carbohydrate chains extending into the aqueous phase generate steric hindrance, whereas the ionized carboxyl groups contribute to electrostatic repulsion between neighboring droplets. Consequently, increasing the surfactant concentration not only enhances interfacial coverage but also promotes the formation of a more cohesive and mechanically resistant interfacial film capable of withstanding the intense disruptive forces generated during ultrasonication (19).

These observations agree well with previous investigations involving QSS-stabilized nanoemulsions. Schreiner *et al.* showed that increasing QSS concentration significantly reduced droplet size while producing highly negative zeta potentials, confirming the strong interfacial activity of this natural biosurfactant (13). Similarly, Schreiner *et al.* later showed that QSS-based nanoemulsions containing α-tocopherol exhibited droplet sizes between 80 and 121 nm, which translated into improved dermal permeation and excellent physicochemical stability. The droplet sizes obtained in the present study therefore fall remarkably close to those previously reported for QSS-stabilized dermal nanoemulsions, further confirming the suitability of this natural surfactant for topical drug delivery (19).

An important finding of the present study is that progressive droplet size reduction alone did not necessarily predict overall nanoemulsion quality. Although increasing the QSS concentration consistently produced smaller droplets, subsequent accelerated stability studies showed that droplet size should be interpreted alongside particle size distribution, zeta potential, and resistance to physical stress. This observation emphasizes that optimizing solely for the smallest possible droplet size may be misleading because long-term colloidal stability depends on multiple physicochemical parameters acting simultaneously. Similar conclusions have been reported for several topical nanoemulsion systems, where formulations exhibiting slightly larger but more homogeneous droplets frequently outperformed those with extremely small yet less uniformly distributed particles during storage and stress testing (17, 42).

From a pharmaceutical perspective, nanoscale droplets provide a large interfacial area and may facilitate close contact between the formulation and the skin surface. However, droplet size alone does not determine enhanced cutaneous penetration, spatial drug distribution, or biological efficacy. These outcomes depend on multiple formulation- and skin-related factors and require direct experimental evaluation. Accordingly, nanoscale droplet dimensions obtained by optimizing QSS concentration should be interpreted primarily as a physicochemical formulation characteristic rather than direct evidence of improved dermal delivery or wound-healing efficacy (5, 39).

The PDI values of the freshly prepared nanoemulsions ranged from 0.171 to 0.390, with all formulations except NE2.3 below 0.30, indicating relatively narrow droplet-size distributions and acceptable colloidal homogeneity. In nanoparticulate systems, PDI values below approximately 0.30 generally indicate a uniform droplet population, which supports reproducible physicochemical behavior during storage and topical application. A narrow size distribution minimizes the coexistence of excessively small and large droplets, thereby reducing the probability of differential creaming, Ostwald ripening, and coalescence while contributing to more predictable drug release and dermal permeation characteristics (17).

Although NE2.3 exhibited one of the smallest mean droplet sizes (76.10 nm), it also showed the highest PDI (0.390), demonstrating that droplet size alone is insufficient to evaluate nanoemulsion quality. A low mean particle size may still represent a heterogeneous system if the droplet population is broadly distributed. Such heterogeneity may compromise long-term physical stability because larger droplets are more susceptible to gravitational separation, whereas smaller droplets may accelerate diffusion-driven destabilization processes. Therefore, evaluating droplet size and PDI together provides a more reliable assessment of nanoemulsion quality than considering either parameter alone.

The relatively low PDI values obtained for the remaining formulations indicate that increasing the QSS concentration promoted not only droplet size reduction but also the formation of a more homogeneous droplet population. This observation is consistent with the rapid adsorption of QSS molecules onto newly generated interfaces during ultrasonication, enabling more uniform stabilization of dispersed droplets. Similar improvements in particle size distribution have been reported for QSS-stabilized nanoemulsions and other topical nanoformulations, where adequate surfactant coverage resulted in homogeneous dispersions with improved physicochemical stability (19).

Overall, the PDI results confirmed that the optimized formulations achieved nanoscale droplet sizes and relatively narrow particle size distributions, indicating successful emulsification and favorable colloidal uniformity. Together with droplet size and stability evaluations, these findings supported the selection of the 0.5% berberine nanoemulsions (NE1.1, NE1.2, and particularly NE1.3) for subsequent nanoemulgel development.

TEM provided complementary morphological information on the selected NE1.3 nanoemulsion that DLS alone could not provide. The micrographs showed predominantly spherical to near-spherical nanodroplets with clearly distinguishable boundaries and no prominent large-scale aggregation in the examined fields. These observations were qualitatively consistent with the nanoscale droplet dimensions determined by DLS for NE1.3. However, direct numerical agreement between TEM and DLS measurements should not be expected because the two techniques characterize particles under different conditions. DLS provides an intensity-weighted hydrodynamic diameter of dispersed structures in the liquid state, whereas TEM directly visualizes droplets after dilution, deposition, negative staining, and drying. Sample preparation for TEM may therefore influence the apparent dimensions and morphology of the droplets. Accordingly, the TEM findings should be considered complementary to, rather than directly interchangeable with, the DLS results. Together, the two techniques provide complementary evidence supporting the nanoscale dispersed structure of the selected NE1.3 formulation.

Since particle size and PDI alone cannot fully predict

Corrected Proof

colloidal stability, the surface electrical properties of the nanoemulsions were further evaluated by zeta potential measurements. All nanoemulsion formulations showed negative zeta potential values ranging from −23.33 to −31.50 mV, reflecting QSS adsorption at the oil-water interface. This negative surface charge primarily arises from ionizable glucuronic acid residues in the hydrophilic carbohydrate chains of QSS, which generate electrostatic repulsion between adjacent droplets and reduce their tendency to aggregate. Similar negative zeta potentials have been consistently reported for QSS-stabilized nanoemulsions, confirming that this natural biosurfactant forms electrically charged interfacial layers that enhance colloidal stability (19).

Except for NE2.1, all formulations exhibited zeta potential values close to or exceeding −30 mV, a threshold frequently associated with improved electrostatic stabilization of colloidal systems. Nevertheless, zeta potential should not be interpreted as an absolute predictor of nanoemulsion stability. Several topical nanoformulations with lower absolute zeta potential values have shown excellent physicochemical stability when steric stabilization from surfactants or polymeric interfacial layers complemented electrostatic repulsion. For example, Ahmad *et al.* reported a curcumin nanoemulsion with a zeta potential of only −11.67 mV (38), while Algahtani *et al.* described a curcumin nanoemulsion with a zeta potential of −20.26 mV (17); despite these comparatively lower values, both formulations remained physically stable and exhibited favorable wound-healing performance. These findings indicate that overall colloidal stability depends on the combined contribution of electrostatic and steric stabilization rather than surface charge alone (17).

In the present study, the negative zeta potentials, along with the favorable droplet size and PDI values, suggest that QSS provided effective electrosteric stabilization at the oil-water interface. Electrostatic stabilization arose from the negatively charged glucuronic acid residues located within the hydrophilic carbohydrate moieties of QSS. In contrast, the protruding oligosaccharide chains extending into the aqueous phase created steric hindrance that prevented droplets from approaching closely. This combination of electrostatic and steric stabilization may therefore have contributed to the optimized nanoemulsions' resistance to droplet aggregation during centrifugation and thermal stress. However, because interfacial organization and specific berberine–QSS interactions were not directly characterized, this mechanistic interpretation should be regarded as a plausible explanation rather than direct experimental evidence (19).

Interestingly, the formulations containing 1.0% berberine did not remain physically stable despite exhibiting relatively small initial droplet sizes and moderately negative zeta potentials. This observation shows that favorable droplet size and surface charge alone were insufficient to ensure formulation robustness when drug loading exceeded the system's physicochemical capacity. Increasing berberine concentration may have altered the continuous-phase ionic environment and partially weakened QSS-provided electrostatic stabilization. Moreover, potential interactions between berberine's positively charged quaternary ammonium group and QSS's negatively charged functional groups may have disrupted optimal surfactant organization at the interface. Although these mechanisms were not directly investigated, they provide plausible explanations for the reduced stress stability observed in the high-drug formulations and warrant further study.

Collectively, the physicochemical characterization showed that increasing QSS concentration reduced droplet size while maintaining relatively narrow particle-size distributions and sufficiently negative surface charges. However, the accelerated stability results clearly indicated that minimizing droplet size alone could not achieve successful nanoemulsion optimization. Instead, formulation selection required the simultaneous consideration of droplet size, PDI, zeta potential, and resistance to physical stress.

Beyond surfactant concentration, drug loading also played a decisive role in formulation stability. Although the nanoemulsions containing 1.0% berberine initially exhibited nanosized droplets, all formulations failed during accelerated stability testing, indicating that increasing drug concentration exceeded the system's stabilization capacity. In contrast, the 0.5% berberine formulations remained physically stable under centrifugation and thermal stress, demonstrating a more favorable balance between drug loading and interfacial stabilization.

Among these formulations, NE1.3, containing 0.5% berberine and 1.0% QSS, exhibited the most balanced physicochemical profile, combining a small mean droplet size (71.18 nm), an acceptable PDI (0.244), a sufficiently negative zeta potential (−30.23 mV), and excellent resistance to centrifugation and thermal stress. These findings indicate that this formulation achieved an appropriate balance between efficient interfacial stabilization and drug loading capacity. Consequently, NE1.3 was selected as the optimized nanoemulsion for subsequent nanoemulgel development.

Overall, the present findings demonstrate that QSS is an effective natural biosurfactant for producing physically stable berberine-loaded nanoemulsions suitable for topical delivery. By simultaneously providing nanoscale droplet dimensions, acceptable colloidal uniformity, and favorable surface charge characteristics, the optimized formulation established a robust physicochemical platform for the subsequent development of a wound-healing nanoemulgel.

Characterization and accelerated stability of berberine-loaded nanoemulgels

In the present study, incorporating the selected berberine-loaded nanoemulsions into xanthan gum hydrogels produced six nanoemulgel formulations while preserving the nanometric character of the dispersed phase, with initial mean droplet sizes ranging from 100.79±11.48 to 238.03±8.22 nm. Preserving nanoscale droplets after converting a nanoemulsion into a semisolid gel is important for maintaining the colloidal characteristics of the dispersed system and its suitability for topical delivery (17, 37). Comparable nanometric dimensions have been reported for topical nanoemulgels, including a xanthan gum-based jackfruit leaf extract system with droplet sizes of approximately 138-230 nm and a dipyridamole–roflumilast nanoemulgel with a particle size of approximately 173 nm after gel formation (37, 42).

Gel incorporation nevertheless produced formulation-dependent changes in droplet size, PDI, and zeta potential compared with the corresponding parent nanoemulsions, demonstrating that conversion into a nanoemulgel was

Corrected Proof

not merely a viscosity-enhancing step but also altered the physicochemical environment surrounding the dispersed droplets. For the NE1.1 and NE1.2 series, incorporation into 1% xanthan gum did not significantly change the mean droplet size, whereas 2% xanthan gum significantly increased it in both series; in the NE1.3 series, both xanthan gum concentrations increased the measured droplet size relative to the parent nanoemulsion. Similar increases after nanoemulsion gelation have been reported for xanthan gum and other anionic gel-forming polymers and have been attributed to polymer adsorption, polymer–surfactant interactions, hydration of the droplet-associated polymer layer, and an increase in the apparent hydrodynamic diameter detected by dynamic light scattering (42, 43).

The larger droplet sizes observed at 2% xanthan gum were therefore not necessarily indicative of droplet coalescence, because all formulations remained within the nanoscale range and retained strongly negative zeta potentials before stress testing. Xanthan gum is a high-molecular-weight anionic polysaccharide whose hydroxyl and carboxyl groups promote extensive hydration, hydrogen bonding, chain association, and formation of a highly viscous three-dimensional network within the aqueous phase (43). Increasing its concentration can thicken the hydration layer surrounding dispersed droplets, increase polymer-chain entanglement, and restrict droplet mobility, all of which may increase the DLS-derived hydrodynamic diameter without necessarily representing irreversible enlargement of the oil cores (42, 43). Mustafa *et al.* similarly reported an increase from approximately 131 nm for the parent nanoemulsion to 138-230 nm after incorporation into xanthan gum-containing gels, with the magnitude of the increase depending on polymer composition and concentration (42).

The initial PDI values ranged from 0.22±0.02 to 0.364±0.007, indicating formulation-dependent differences in droplet population uniformity after gel formation. The values close to 0.22 obtained for NE1.3 containing either 1% or 2% xanthan gum and for NE1.2 containing 2% xanthan gum represented comparatively narrow distributions, whereas the values of approximately 0.35-0.36 observed for NEJ1.1 and NEJ1.2 containing 1% xanthan gum reflected broader, although still measurable, droplet populations. Nanoemulgels generally exhibit broader size distributions than their parent nanoemulsions because diluting and dispersing the polymeric gel before DLS analysis can release droplets along with polymer-associated structures or weak droplet clusters with different hydrodynamic dimensions (42, 43). Accordingly, Mustafa *et al.* observed PDI values of approximately 0.25-0.33 after gelation of a nanoemulsion with xanthan gum-containing matrices, compared with approximately 0.23 for the parent nanoemulsion (42).

The influence of gel formation on PDI also depended on the parent nanoemulsion composition, because PDI increased significantly in the NE1.1 and NE1.2 series but remained statistically unchanged between NE1.3 and its corresponding nanoemulgels. This finding suggests that the NE1.3 interfacial film, formed using the highest QSS concentration among the selected nanoemulsions, was more resistant to perturbation during incorporation into xanthan gum than those of the NE1.1 and NE1.2 systems. QSS can provide both electrostatic stabilization through its ionizable acidic groups and steric stabilization through carbohydrate chains extending into the aqueous phase. At the same time, the surrounding xanthan gum network can further restrict droplet movement and collision (19, 42). The absence of a significant PDI increase in the NE1.3 series may therefore reflect a favorable compatibility between the saponin-stabilized interface and the xanthan gum-rich continuous phase (19).

All freshly prepared nanoemulgels exhibited strongly negative zeta potentials ranging from −32.50±1.55 to -43.00±1.25 mV, indicating that the dispersed droplets retained a substantial negative surface charge after gel incorporation. Nanoemulgel formation generally shifted the zeta potential toward more negative values, particularly in the NE1.1 and NE1.3 series and in NEJ1.2 containing 2% xanthan gum. This behavior is consistent with the anionic character of xanthan gum, whose glucuronic acid and pyruvate-containing side chains introduce negatively charged groups into the droplet-associated polymeric environment (42, 43). Mustafa *et al.* likewise reported that increasing xanthan gum content shifted zeta potential from approximately -27 mV in the parent nanoemulsion to values between approximately -31 and -47 mV in the corresponding nanoemulgels (42).

The strongly negative zeta potentials obtained in the present study indicate that xanthan gum complemented the negative interfacial charge already provided by QSS rather than neutralizing it. This combined contribution may enhance electrosteric stabilization by increasing electrostatic repulsion, while the hydrated polysaccharide chains simultaneously create a steric barrier against close droplet approach (19, 42). Nevertheless, zeta potential alone cannot establish complete physical stability in a highly structured nanoemulgel, because polymer-network integrity, droplet distribution, viscosity, interfacial composition, and resistance to external stress also influence formulation behavior (17, 43).

Accelerated stability testing further showed that nanoemulgel response depended on both the parent nanoemulsion and xanthan gum concentration. Centrifugation increased the apparent droplet size of NEJ1.1 and NEJ1.2 containing either 1% or 2% xanthan gum, whereas it reduced the measured size of both NEJ1.3 formulations. Centrifugal stress can increase droplet contact frequency, compress or rearrange the polymeric network, and promote reversible droplet association or polymer bridging, which may appear as an increase in hydrodynamic diameter after sample dilution (43). Conversely, a decrease in measured size after centrifugation may arise from disruption of weak droplet clusters, redistribution of the dispersed phase, or altered droplet release from the gel network during dilution rather than from actual fragmentation of the oil droplets (43).

The centrifugation results therefore require interpreting droplet size, PDI, and zeta potential together rather than relying on size alone. In NEJ1.3 containing 2% xanthan gum, droplet size decreased from 188.93±5.13 to 159.73±5.36 nm after centrifugation, while the PDI remained unchanged at approximately 0.224 and the zeta potential also remained statistically stable. This combination suggests redistribution of the nanodroplets within the xanthan gum matrix without a detectable loss of population uniformity or interfacial charge. In contrast, the marked PDI increase observed after centrifugation in NEJ1.3 containing 1% xanthan gum, from 0.232±0.016 to 0.491±0.005, indicates that the lower-

Corrected Proof

polymer matrix was less able to preserve a uniform droplet population under centrifugal stress.

Thermal stress produced more pronounced alterations than centrifugation in most formulations, particularly in the PDI values. NEJ1.1 and NEJ1.2 containing 1% xanthan gum showed post-thermal PDI values of 0.506 and 0.466, respectively, while their corresponding 2% xanthan gum formulations reached 0.775 and 0.537. Elevated temperature can increase molecular mobility, weaken hydrogen bonding, modify xanthan chain conformation, alter polymer–surfactant interactions, and rearrange the QSS-containing interfacial layer surrounding the droplets (19, 43). These changes can generate a heterogeneous mixture of individually dispersed droplets, partially associated droplets, and polymer-associated structures, thereby broadening the size distribution measured after thermal exposure (43).

The substantial decrease in mean droplet size observed after thermal stress in several nanoemulgel formulations should not be interpreted as a true uniform shrinkage of the oil droplets or as an improvement in physical stability, because the decrease in mean size generally coincided with a considerable increase in PDI. For example, NEJ1.1 containing 2% xanthan gum decreased from 238.03±8.22 to 78.60±5.67 nm after thermal stress, while its PDI increased markedly from 0.346±0.015 to 0.775±0.064. Similarly, NEJ1.2 containing 2% xanthan gum decreased from 221.57±5.87 to 81.77±7.79 nm, while its PDI increased from 0.223±0.020 to 0.537±0.012. Thus, the lower arithmetic mean hydrodynamic diameter was associated with a substantially broader, more heterogeneous size distribution rather than the formation of a uniformly smaller droplet population. Moreover, because the nanoemulgels were diluted before DLS analysis, thermal modification of the gel network may have altered the way droplets, weak droplet aggregates, and polymer-associated structures were released or dispersed during sample preparation, thereby influencing the measured hydrodynamic size (43). Consequently, the apparent reduction in mean hydrodynamic diameter may partly reflect changes in the particle population detected by DLS after dilution rather than actual thermal shrinkage of individual oil droplets. Therefore, a contribution from sample-preparation- and DLS-related measurement effects cannot be excluded.

The post-stress zeta-potential changes were generally less pronounced than changes in droplet size and PDI, suggesting that the negative interfacial character was retained even as the droplet distribution broadened. Several 1% xanthan gum formulations became significantly less negative after stress, which may indicate partial rearrangement or displacement of anionic polymer and saponin molecules near the droplet interface (19). By contrast, NEJ1.2 and NEJ1.3 containing 2% xanthan gum showed no statistically significant zeta-potential changes after centrifugation or thermal stress, suggesting that the denser xanthan gum matrix may have better preserved the electrokinetic environment of the dispersed phase under the tested conditions. The higher polymer concentration may have limited droplet mobility and provided an additional steric barrier. However, the marked PDI increases in NEJ1.1 and NEJ1.2 demonstrate that surface charge preservation alone was insufficient to prevent thermal heterogeneity.

Among the six formulations, NEJ1.3 containing 2% xanthan gum exhibited the most balanced overall physicochemical and accelerated-stability profile. This formulation initially combined a nanometric droplet size of 188.93±5.13 nm, a low PDI of 0.224±0.010, and a strongly negative zeta potential of -40.37±1.94 mV. Its PDI remained unchanged after centrifugation and increased only moderately to 0.323±0.013 after thermal stress, whereas its zeta potential did not change significantly under either condition. Although the post-thermal PDI slightly exceeded the commonly used approximate value of 0.30, the increase was considerably smaller than that observed for NEJ1.1 and NEJ1.2, which reached values between 0.466 and 0.775.

The comparatively favorable behavior of NEJ1.3 containing 2% xanthan gum may be attributed to the combined contribution of a robust parent nanoemulsion interface and a sufficiently dense xanthan gum network. The parent NE1.3 formulation contained the highest QSS concentration and had already demonstrated a small initial droplet size, acceptable PDI, and resistance to accelerated stress before gel incorporation. The 2% xanthan gum phase then provided increased viscosity, greater chain entanglement, and reduced droplet mobility, while its anionic groups reinforced the negative surface environment generated by QSS (19, 42). Similar findings show that nanoemulgels with higher xanthan gum proportions can display stronger rheological structure and better physical stability than systems with insufficient polymer concentrations (42).

Overall, these findings show that successful nanoemulgel optimization cannot be based solely on achieving the smallest mean droplet size. The most informative assessment required simultaneous consideration of initial droplet size, PDI, zeta potential, changes after centrifugation and thermal stress, and the magnitude of stress-induced broadening of the droplet distribution. On this basis, NEJ1.3 containing 2% xanthan gum provided the best compromise among preservation of nanoscale structure, droplet population uniformity, negative interfacial charge, and resistance to accelerated stress. It was therefore selected for subsequent physicochemical, mechanical, release, permeation, storage-stability, and biological evaluations.

Physicochemical stability: pH and electrical conductivity

The optimized nanoemulgel (NEJ1.3 containing 2% xanthan gum and 0.5% berberine) exhibited an initial pH of 4.42, which gradually decreased during the three-month storage period under all storage conditions. Nevertheless, the observed reduction was relatively small, and the formulation maintained a mildly acidic pH within the physiologically acceptable range for topical application throughout the study. Maintaining an acidic pH is particularly advantageous for wound-healing formulations, as it closely resembles the natural skin surface pH (approximately 4.5-5.5), thereby preserving skin barrier function, reducing the risk of irritation, inhibiting the growth of pathogenic microorganisms, promoting oxygen release from hemoglobin, and supporting enzymatic processes involved in tissue repair (44).

The slight decrease in pH observed during storage may be attributed to gradual physicochemical changes occurring within the nanoemulgel matrix rather than substantial chemical degradation of the formulation. During storage, slow hydrolytic processes, minor rearrangement of the xanthan gum polymer network, and subtle changes at the

Corrected Proof

oil-water interface may contribute to small shifts in hydrogen ion concentration. However, the relatively small pH changes observed during storage suggest that the formulation's acid-base characteristics did not change significantly over the evaluated period. Nevertheless, pH monitoring alone cannot establish chemical stability or exclude degradation of individual formulation components. Moreover, the electrosterically stabilized nanoemulsion droplets, together with the three-dimensional xanthan gum matrix, likely helped maintain a chemically stable microenvironment throughout storage.

Similar findings have been reported for xanthan gum-based nanoemulgels and other polysaccharide-containing topical delivery systems. Mustafa *et al.* reported that nanoemulgels prepared with xanthan gum retained skin-compatible pH values during storage despite slight decreases over time (42), while Mahdi *et al.* likewise observed only minor pH fluctuations that did not compromise formulation suitability for dermal application (45). Comparable behavior has also been described for polysaccharide-based nanoemulgels, where small pH reductions are generally attributed to gradual physicochemical equilibration of the polymeric network rather than extensive degradation of formulation components. Therefore, the pH profile observed in the present study demonstrates good physicochemical stability and remains fully compatible with topical wound-healing applications (42).

The electrical conductivity profile of the optimized nanoemulgel further supported its physicochemical stability during storage. Conductivity values remained relatively constant under all storage conditions throughout the three-month study, indicating that the formulation's ionic characteristics were well preserved. Because electrical conductivity reflects ion mobility within the continuous aqueous phase, stable conductivity values suggest no substantial changes in the nanoemulgel's internal structure, such as phase separation, disruption of the polymer network, or degradation of formulation components.

These findings align with previous reports on xanthan gum-based and other polysaccharide-containing nanoemulgels, where electrical conductivity remained largely unchanged during storage, reflecting preserved formulation microstructure and ionic balance (42). Therefore, the stable conductivity profile observed in the present study provides additional evidence that the optimized nanoemulgel maintained its physicochemical integrity throughout storage, supporting its suitability as a stable topical drug delivery system.

Rheological behavior and storage stability of the optimized nanoemulgel

The optimized berberine-loaded nanoemulgel exhibited a typical non-Newtonian pseudoplastic (shear-thinning) flow behavior, as demonstrated by the progressive decrease in viscosity with increasing shear rate and the excellent fit of the experimental data to the Power Law model (R^2=0.9979). The low flow behavior index (n=0.289) confirms pronounced shear-thinning, indicating that viscosity decreases under mechanical stress and recovers after the applied force is removed. This rheological behavior is highly desirable for topical formulations because it facilitates spreading during application while allowing the formulation to regain viscosity afterward, improving residence time at the application site and minimizing runoff (46, 47).

The observed rheological profile is primarily attributed to the structural characteristics of xanthan gum. Xanthan gum is a high-molecular-weight anionic polysaccharide that forms an interconnected three-dimensional network through intermolecular hydrogen bonding and physical chain entanglement. At low shear rates, this network remains intact, producing relatively high viscosity. As shear rate increases, progressive disruption and alignment of polymer chains in the direction of flow reduce internal resistance, leading to the characteristic decrease in viscosity. When shear is removed, the weak non-covalent interactions between xanthan gum molecules allow partial reconstruction of the polymer network, enabling recovery of the gel structure (46, 48). Such shear-thinning behavior is advantageous for topical application because reduced viscosity under shear facilitates spreading, whereas viscosity recovery after application may support formulation retention at the application site (47, 48). The rheological parameters obtained in the present study are consistent with previous reports describing nanoemulgels intended for topical application. Mustafa *et al.* demonstrated that increasing xanthan gum concentration markedly increased the consistency index while reducing the flow behavior index to approximately 0.12-0.14, confirming pronounced pseudoplastic flow. Similarly, Saab *et al.* reported a flow behavior index of 0.13 for a capsaicin-loaded nanoemulgel. Collectively, these findings support the suitability of xanthan gum-containing nanoemulgels for achieving pseudoplastic rheological characteristics appropriate for topical application (42, 47). Storage studies further demonstrated that the optimized nanoemulgel maintained its characteristic shear-thinning behavior throughout the three-month evaluation period under refrigerated, room-temperature, and accelerated storage conditions. Under refrigerated and room-temperature storage, viscosity changed only minimally. Although accelerated storage moderately reduced viscosity, the overall rheological profile was preserved, and the formulation continued to exhibit pronounced pseudoplastic flow. This suggests that elevated temperature caused partial relaxation or rearrangement of the polymer network rather than irreversible structural degradation or loss of gel integrity.

The moderate viscosity reduction observed under accelerated conditions is consistent with the temperature-dependent behavior of xanthan gum. Elevated temperatures increase molecular mobility, weaken intermolecular hydrogen bonding, and promote partial relaxation of polymer chain entanglements, reducing the gel matrix's resistance to deformation (46). Nevertheless, the persistence of shear-thinning behavior throughout storage indicates that the nanoemulgel's functional rheological characteristics were preserved despite the reduction in absolute viscosity. Comparable rheological behavior has been reported for xanthan gum-containing semisolid systems, in which the polymeric network contributes to viscosity and shear-thinning characteristics (42, 46)

From a pharmaceutical perspective, preserving pseudoplastic behavior during storage is important for topical wound-healing systems. An optimal rheological profile ensures convenient dispensing and uniform spreading during application while maintaining adequate viscosity after administration to prolong contact with the wound

Corrected Proof

surface. Prolonged residence time may improve local drug availability, reduce formulation loss from the application site, and support sustained therapeutic action. Furthermore, xanthan gum-based hydrogels have been shown to provide favorable mechanical strength, bioadhesion, and controlled drug release, all of which contribute to an environment conducive to wound repair (49).

Mechanical properties and spreadability of the optimized nanoemulgel

The optimized berberine-loaded nanoemulgel exhibited higher hardness than the conventional gel, with values of 11.66±0.13 and 7.59±0.10 g, respectively. This finding indicates that incorporating the nanoemulsion into the 2% xanthan gum matrix produced a mechanically stronger, more deformation-resistant semisolid structure. Hardness represents the maximum force required to deform a formulation during the first compression cycle and is closely related to polymer concentration, network density, and consistency (50, 51). The increased hardness of the nanoemulgel may therefore be attributed to the high molecular weight of xanthan gum and the formation of an associated polymeric network through chain entanglement and intermolecular interactions, which can increase resistance to deformation (42, 46).

The higher hardness of the nanoemulgel may also reflect the combined contribution of the xanthan gum matrix and the dispersed nanoemulsion phase to the overall semisolid structure. Consistent with this interpretation, Mustafa *et al.* reported increased viscosity and pronounced rheological characteristics in xanthan gum-containing nanoemulsion gels as the polymer concentration increased (42).

In texture profile analysis, adhesiveness represents the work required to overcome the attractive forces between the formulation and the probe surface during withdrawal; therefore, a greater magnitude of negative adhesiveness reflects stronger adhesive interaction (50). The greater adhesiveness of the nanoemulgel may be associated with the hydrophilic and polymeric characteristics of xanthan gum, which can promote intermolecular interactions and contribute to the gel matrix's adhesive behavior (46). For a topical wound-healing formulation, adequate adhesiveness may be advantageous by supporting prolonged residence and closer contact between the formulation and the application site. However, adhesiveness should remain balanced because excessive adhesion may impair ease of application or removal (50, 51). In the present study, therefore, higher adhesiveness should be interpreted alongside the nanoemulgel's favorable shear-thinning behavior and springiness rather than as an isolated property. The conventional gel showed slightly higher cohesiveness than the nanoemulgel, with values of 0.880±0.027 and 0.839±0.042, respectively. Cohesiveness reflects a formulation's ability to withstand repeated deformation and is commonly derived from the relationship between the areas under successive compression cycles (50). Although the nanoemulgel exhibited a modestly lower value, its cohesiveness remained high and therefore indicated preservation of substantial internal structural integrity. The slight reduction may be associated with incorporation of nanodroplets into the xanthan gum matrix, creating a heterogeneous biphasic microstructure that may permit localized rearrangement or partial disruption of polymer associations during repeated compression. Thus, the lower cohesiveness does not necessarily indicate poor formulation quality but rather a somewhat greater capacity to dissipate mechanical stress.

Springiness reflects a formulation's ability to recover its structure between successive deformation cycles, whereas resilience describes immediate elastic recovery during the first compression cycle (50). The near-unity springiness of the nanoemulgel therefore indicates substantial structural recovery between successive compression cycles, whereas its lower resilience suggests less immediate elastic recovery than the conventional gel. Consistent with this interpretation, resilience was lower for the nanoemulgel than for the conventional gel (0.127±0.005 vs. 0.271±0.017, respectively).

Firmness reflects the force required to initiate spreading or deformation, whereas work of shear represents the energy required to spread the sample. Accordingly, the higher values observed for the nanoemulgel indicate greater resistance to spreading under the test conditions (51). These findings are consistent with the nanoemulgel's higher hardness and adhesiveness and further support the formation of a dense xanthan gum-based three-dimensional network.

Although increased firmness and work of shear indicate that the nanoemulgel is less readily spread than the conventional gel under static test conditions, this should not automatically be regarded as unfavorable. Topical semisolid formulations require a balance between ease of spreading and sufficient consistency for retention at the application site. Increasing xanthan gum concentration can increase the structural consistency of the gel matrix and consequently increase resistance to spreading (42, 46). In the present formulation, the higher work of shear is therefore consistent with the 2% xanthan gum concentration and the greater mechanical strength of the nanoemulgel.

Importantly, the shear-thinning behavior of the optimized nanoemulgel may partly compensate for its relatively high static firmness. Under shear, polymer-chain alignment reduces apparent viscosity and can facilitate spreading, whereas viscosity recovery after shear removal may support retention at the application site. Such rheological behavior, combined with appropriate firmness and adhesiveness, is desirable for topical semisolid formulations (48, 51). Overall, the nanoemulgel's mechanical profile indicates greater hardness, adhesiveness, firmness, and resistance to spreading than the conventional gel, while maintaining pronounced shear-thinning behavior. These characteristics support its suitability as a semisolid system for localized topical application. Similar wound-healing nanoemulgel and berberine-containing gel systems have demonstrated favorable properties for topical drug delivery (17, 52).

The semisolid nature of topical nanoemulgels may potentially influence the local skin environment through surface occlusion and hydration. However, the present study did not directly evaluate occlusivity or skin hydration. Therefore, the current data cannot establish the contribution of these parameters to the observed formulation performance, and no mechanistic conclusions regarding occlusive or hydration-mediated effects can be drawn.

In vitro drug release behavior

The three formulations exhibited distinct release profiles, indicating that formulation architecture influenced berberine release. At 24 hr, the conventional gel showed

Corrected Proof

the highest cumulative release (87.93±3.01%), followed by the nanoemulsion (68.19±2.59%) and the optimized nanoemulgel (63.22±2.25%). The faster release from the conventional gel may be due to greater berberine availability within the hydrated gel matrix and the absence of an oil-phase reservoir. In contrast to nanoemulsion-based systems, the conventional gel does not require an additional drug-partitioning step from dispersed oil droplets before diffusion through the release medium. Similar sustained-release behavior has been described for xanthan gum-based drug-delivery systems and berberine-containing polymeric wound-healing formulations (43, 52). Compared with the conventional gel, the nanoemulsion showed a slower release profile, indicating that incorporating berberine chloride into the nanoemulsion system did not necessarily accelerate drug release. The dispersed oil phase may act as a drug reservoir, requiring berberine associated with the droplets to partition into the external aqueous phase before diffusing across the membrane. This additional partitioning step may contribute to the more gradual release profile observed for the nanoemulsion (37). The optimized nanoemulgel showed the slowest release profile, which may reflect the combined diffusional resistance of the dispersed nanoemulsion phase and the 2% xanthan gum matrix. Xanthan gum forms a hydrated polymeric network through intermolecular interactions and chain entanglement, increasing matrix viscosity and potentially creating a more tortuous pathway for drug diffusion. Incorporation of nanoemulsion droplets into this polymeric matrix may therefore provide an additional diffusional barrier to berberine release (43, 46). Consistent with this interpretation, Mustafa *et al.* reported that increasing xanthan gum concentration increased the consistency of xanthan gum-containing nanoemulsion gels, while xanthan gum-based drug-delivery systems have been described as matrices capable of modulating drug release (42, 43).

Overall, the observed release order (conventional gel>nanoemulsion>nanoemulgel) is consistent with the progressive introduction of additional diffusional barriers within the formulation systems. The nanoemulsion introduced a potential droplet-mediated partitioning step, whereas incorporation into the xanthan gum matrix added another potential barrier to drug diffusion. Together, these formulation features may therefore provide complementary control over berberine release, consistent with the established role of polymeric matrices in sustained drug-delivery systems (37, 43, 53).

The dialysis membrane-based Franz diffusion cell method used in the present study is a commonly employed approach for comparative *in vitro* release assessment of semisolid and nanoformulated delivery systems. Nevertheless, the dialysis membrane adds a diffusional barrier between the formulation and the receptor medium. Therefore, the measured release profiles represent the combined processes of berberine release from the formulation and subsequent diffusion across the dialysis membrane, rather than an unrestricted measure of intrinsic drug release from the formulation alone. Accordingly, the present release data should primarily be interpreted comparatively among formulations tested under identical experimental conditions. The slower apparent release observed from the nanoemulgel may reflect the influence of formulation architecture on berberine transport under these test conditions; however, a potential contribution of membrane-controlled diffusion cannot be excluded.

Drug release kinetics

Among the evaluated kinetic models, the Korsmeyer–Peppas model provided the highest R^2 values for all three formulations, suggesting that berberine release may involve more than a single diffusion-controlled process. For the nanoemulgel and nanoemulsion, the Korsmeyer–Peppas model yielded R^2 values of 0.9995 and 0.9984, with release exponent (n) values of 0.759 and 0.824, respectively. These values suggest contributions from more than one transport process; however, mechanistic interpretation of the release exponent should be made cautiously because it depends on the delivery system's geometry and characteristics. In the nanoemulgel, this behavior may be related to the hydrated xanthan gum matrix, which can increase diffusional resistance and modulate drug release. Comparable sustained-release behavior has been described for xanthan gum-based drug-delivery systems and berberine-containing polymeric wound-healing formulations (43, 52). The conventional gel exhibited an n value of 1.128, indicating a release pattern different from those of the nanoemulsion and nanoemulgel. However, this value should not be interpreted as evidence of a specific release mechanism in isolation. Accordingly, the Korsmeyer–Peppas parameters should be interpreted cautiously in these semisolid systems, and the obtained n values are better considered supportive indicators of release behavior than definitive evidence of a single release mechanism.

The Higuchi model showed the second-highest R^2 values for the nanoemulgel (0.972) and nanoemulsion (0.938), supporting diffusion as a major contributor to berberine release from these formulations. The lower Higuchi release constant for the nanoemulgel (kH=96.09) than for the nanoemulsion (104.64) and conventional gel (116.49) is consistent with slower diffusional release from the xanthan gum-containing nanoemulgel. The slower release observed from the nanoemulgel is also consistent with the rheological characteristics of the xanthan gum matrix. Increasing xanthan gum concentration can increase matrix viscosity and structural consistency, thereby increasing resistance to drug diffusion. Similar relationships between xanthan gum content, matrix properties, and drug-release behavior have been reported in xanthan gum-containing delivery systems (42, 43). Overall, the kinetic findings support a more sustained release profile for the nanoemulgel, consistent with the combined influence of the nanoemulsion phase and the xanthan gum matrix on berberine diffusion.

Ex vivo skin permeation and skin deposition

Ex vivo permeation experiments showed that the nanoemulsion had the highest mean amount detected in the receptor compartment (0.739±0.450 μg/cm^2). In contrast, the nanoemulgel showed the highest mean skin deposition (44.014±6.865 μg/cm^2) among the tested formulations. Because no statistical comparisons were performed among the formulations, interpret these differences descriptively. The observed distribution pattern is consistent with a higher mean amount of berberine recovered from the skin after nanoemulgel application; however, the present *ex vivo* data do not establish the mechanism, penetration pathway, or anatomical localization responsible for this observation.

Corrected Proof

Because imaging techniques such as confocal laser scanning microscopy (CLSM) or fluorescence imaging were not employed, the present findings should not be interpreted as direct evidence of enhanced penetration into specific skin layers or of a particular skin-delivery mechanism. The higher mean permeation observed with the nanoemulsion may be related to its nanosized droplets and the presence of surfactant/cosurfactant components, which can influence drug partitioning and facilitate interactions with the skin barrier (37, 47).

Although the nanoemulgel showed a lower mean amount of berberine in the receptor compartment than the nanoemulsion, it exhibited the highest mean skin deposition among the tested formulations. This descriptive distribution pattern suggests that formulation composition may influence the relative distribution of berberine between the skin and receptor compartment. However, the present study was not designed to determine the mechanisms underlying this distribution. Factors such as formulation viscosity, surface residence, drug release, and interactions between the nanoemulsion and the skin may potentially contribute to the observed pattern. Still, their individual contributions were not experimentally investigated. Therefore, these data do not establish a specific mechanism for enhanced skin penetration or retention (37, 43, 47). This interpretation is consistent with the observed *ex vivo* distribution pattern, in which the nanoemulgel showed a higher mean amount of berberine retained within the skin than recovered in the receptor compartment. From a topical drug-delivery perspective, the higher mean amount of berberine recovered from the skin after nanoemulgel application may support localized delivery. However, because the spatial distribution of berberine within the skin was not determined, the present findings cannot establish whether the drug preferentially accumulated in specific skin layers or at a particular site of topical action. Nanoemulgel and berberine-containing gel systems have previously been investigated as localized delivery platforms for wound-related applications (17, 52).

These findings also provide experimental context for selecting the nanoemulsion–nanoemulgel approach over a conventional hydrogel alone. Whereas the conventional gel primarily provides a hydrated polymeric matrix for topical application, incorporation of the nanoemulsion adds a dispersed phase that can influence drug partitioning, release, and skin interactions. The present study was not designed to compare the nanoemulgel directly with other nanocarrier platforms such as liposomes, SLNs, or NLCs; therefore, no conclusion regarding superiority over these systems can be drawn. Rather, these findings support combining a QSS-stabilized nanoscale dispersion with a xanthan gum matrix to integrate formulation-dependent modulation of berberine release and skin distribution with the application and residence properties of a semisolid hydrogel.

Drug content stability of the optimized nanoemulgel

The optimized berberine-loaded nanoemulgel maintained approximately 100% of its initial drug content throughout three months of refrigerated storage. In contrast, storage at 25 °C showed decreased drug retention after the first month, with approximately 86% of the initial content remaining at months 2 and 3. These findings indicate temperature-dependent differences in berberine retention under the evaluated storage conditions and support refrigerated storage as better for preserving drug content during the three-month study period. The reduced drug retention observed at room temperature is consistent with berberine's known physicochemical instability. Berberine hydrochloride has been shown to undergo photodegradation under simulated sunlight, and comprehensive reviews have discussed its broader pharmacokinetic and physicochemical limitations (54, 55). Encapsulation within the nanoemulsion phase may have contributed to berberine retention by providing a microenvironment that reduces the drug's direct exposure to the external aqueous phase. However, this study did not investigate specific degradation pathways. Berberine has previously been incorporated into nanoemulsion-based delivery systems, supporting the feasibility of lipid-based nanocarriers for improving its pharmaceutical formulation characteristics (56). Researchers have also investigated carrier-based approaches to address berberine's delivery limitations, including transdermal nanocarrier systems (57). The xanthan gum matrix may also have contributed to formulation stability by increasing viscosity and restricting droplet mobility within the continuous phase. Xanthan gum is widely used as a pharmaceutical structuring polymer, and xanthan-containing nanoemulsion gels have demonstrated favorable physicochemical stability (42, 46).

Better preservation of drug content at 4 °C may be associated with reduced molecular mobility and slower degradation at lower temperatures. Improved stability under refrigerated storage has also been reported for berberine-loaded transdermal nanocarrier systems (57). Overall, refrigerated storage better preserved berberine content than storage at 25 °C over the three-month study period. Longer-term stability studies are needed to establish the formulation's shelf life and recommended storage conditions.

Cytocompatibility

HaCaT cell viability generally decreased with increasing formulation concentration, although the magnitude of this response differed among the formulations. All tested systems maintained mean cell viability above 80% at concentrations from 0.78125 to 6.25 mg/ml and at or above 70% up to 12.5 mg/ml. According to the ISO 10993-5 criterion commonly used in *in vitro* cytotoxicity assessment, a reduction in cell viability of more than 30% relative to the untreated control indicates a cytotoxic effect. Accordingly, the viability values observed up to 12.5 mg/ml were consistent with an acceptable *in vitro* cytocompatibility profile under the present experimental conditions (58, 59). Nevertheless, this threshold should be interpreted in relation to the tested concentration and experimental conditions and should not be regarded as evidence of clinical safety or *in vivo* biocompatibility.

The significant formulation×concentration interaction indicates that the effect of formulation composition on cell viability depended on the tested concentration. At 12.5 mg/ml, the nanoemulgel showed significantly higher cell viability than the nanoemulsion, free berberine, and conventional gel. This finding indicates that the nanoemulgel was better tolerated by HaCaT cells than the other tested formulations at this concentration. Nanoencapsulation may modify the fraction of active compound immediately available to cells and thereby influence concentration-dependent cellular responses. Berberine-loaded lipid nanocarriers and other

Corrected Proof

topical nanoemulsion systems have shown favorable compatibility with HaCaT keratinocytes (39, 60). At 25 mg/ml, cell viability did not differ significantly among free berberine, the nanoemulsion, and the nanoemulgel, whereas the conventional gel showed significantly lower viability than each group. A similar pattern was observed at 50 mg/ml, where free berberine, the nanoemulsion, and the nanoemulgel remained statistically comparable, while the conventional gel again showed significantly lower viability. The lower viability observed with the conventional gel at higher concentrations may reflect differences in drug presentation and release from the formulation matrix. However, this cytocompatibility experiment was not designed to determine the mechanism behind these formulation-dependent differences. Furthermore, because the cytocompatibility comparison did not include corresponding blank nanoemulsion and blank gel controls, the respective contributions of formulation excipients and berberine release behavior to the observed differences cannot be distinguished conclusively.

The favorable behavior of the nanoemulgel may also be supported by the generally suitable biological properties of xanthan gum-based systems. Researchers have investigated xanthan gum-containing hydrogels for wound-healing applications, and xanthan gum is widely used as a matrix-forming material in therapeutic delivery systems (61, 62). These reports support the suitability of xanthan gum as a matrix-forming component in topical delivery systems; however, the current experimental design cannot determine its independent contribution to the cytocompatibility of the present formulation.

Overall, the MTT results indicate that the berberine-loaded nanoemulgel was well tolerated by HaCaT keratinocytes at concentrations up to 12.5 mg/ml and showed significantly higher cell viability than the other tested formulations at 12.5 mg/ml. The formulation-dependent differences observed at higher concentrations warrant consideration in future studies, including appropriate blank formulation controls. These findings support further evaluation of the nanoemulgel in additional biocompatibility and *in vivo* wound-healing studies.

***In vitro* scratch closure**

Keratinocyte migration is an important component of re-epithelialization during wound repair. However, the scratch assay primarily evaluates *in vitro* scratch closure associated with cell migration and potentially proliferation and does not reproduce the complex physiological process of wound healing *in vivo*. In the present scratch assay, free berberine significantly increased HaCaT scratch closure from 2.33±3.08% in the negative control to 25.56±4.29% after 24 hr (P=0.0006), indicating a measurable effect of berberine on *in vitro* scratch closure under the tested conditions. Berberine has been reported to modulate keratinocyte proliferation through JAK/STAT3-related signaling, suggesting it can directly influence keratinocyte responses (63). Although the literature has widely reported berberine's anti-inflammatory properties (49), the present study did not evaluate inflammatory biomarkers or molecular mediators. Therefore, the current findings do not provide direct evidence of an anti-inflammatory effect of the developed nanoemulgel, and the observed *in vitro* scratch-closure response should not be mechanistically attributed this potential mechanism directly, future studies should evaluate inflammatory mediators (TNF-α, IL-6, and IL-1β).

The berberine-loaded nanoemulgel achieved 76.33±3.43% scratch closure after 24 hr, significantly higher than both free berberine and the negative control (P<0.0001). Under the same experimental conditions, the mean scratch-closure value of the nanoemulgel was approximately threefold higher than that of free berberine. The greater *in vitro* scratch closure observed with the nanoemulgel may reflect formulation-dependent differences in berberine presentation and release. The nanoemulgel's sustained-release behavior may have helped maintain berberine exposure during the 24 hr assay; however, this study did not directly investigate the cellular mechanisms behind the enhanced scratch closure. The sustained-release and cytocompatibility findings obtained in the present study provide complementary evidence that formulation characteristics may influence cellular exposure to berberine. Nevertheless, the current experiments cannot establish a direct relationship between release kinetics and the observed increase in scratch closure. These findings also align with previous studies showing the wound-healing activity of berberine incorporated into nanostructured wound-delivery systems. Berberine-containing nanofibrous dressings and nanoparticle-based formulations have shown favorable effects on wound repair in experimental models (4, 5, 64).

The xanthan gum matrix may also contribute useful structural properties to a wound-oriented topical formulation. Xanthan gum-based hydrogels have demonstrated favorable wound-healing performance in experimental models, supporting the suitability of this polymer for wound-related delivery systems (49). Nanoemulgel systems developed for wound-related applications have similarly used polymeric gel matrices to combine semisolid application properties with controlled delivery of incorporated bioactive compounds (16). However, because the scratch assay did not include a composition-matched placebo nanoemulgel, the present data cannot distinguish the relative contributions of berberine and the formulation excipients to the observed scratch-closure response. Therefore, the nanoemulgel excipients may have contributed to the observed cellular response. Accordingly, the greater scratch closure observed with the berberine-loaded nanoemulgel should be interpreted as an effect of the complete formulation rather than as a berberine-specific effect.

Overall, the scratch-assay findings demonstrate that the berberine-loaded nanoemulgel produced significantly greater *in vitro* scratch closure than free berberine under the tested conditions. However, because a composition-matched placebo nanoemulgel was not evaluated, the observed response cannot be attributed specifically to berberine, and the formulation vehicle's contribution cannot be excluded.

The biological evaluation in the present study was restricted to HaCaT keratinocytes. Keratinocytes represent an important component of epidermal repair and are therefore useful for preliminary assessment of formulation cytocompatibility and scratch closure. However, cutaneous wound repair is a multicellular process, and dermal fibroblasts have essential roles in extracellular matrix deposition, wound contraction, and tissue remodeling. Therefore, the present HaCaT-based findings represent only the keratinocyte component of the wound-repair response

Corrected Proof

and should not be extrapolated to the overall wound-healing process. Evaluation using NIH-3T3 fibroblasts or, preferably, primary human dermal fibroblasts would provide complementary evidence regarding the effects of the nanoemulgel on the dermal cellular component of wound repair.

Although the nanoemulgel showed acceptable cytocompatibility toward HaCaT keratinocytes under the tested *in vitro* conditions, these findings do not necessarily translate to topical skin safety. The present study did not include dedicated assessments of irritation or other local skin reactions following topical exposure. Therefore, the current data cannot establish the local tolerability and irritation potential of the developed nanoemulgel. Further evaluation using validated topical safety approaches, such as reconstructed human epidermis-based skin irritation models, followed by complementary in vivo or clinically relevant tolerability studies where appropriate, will be necessary before concluding topical safety.

Together with its sustained-release profile and acceptable cytocompatibility, these findings support further investigation of the complete nanoemulgel formulation as a topical berberine delivery system for wound-related applications. Future studies incorporating a composition-matched placebo nanoemulgel, fibroblast-based evaluation, more complex wound models, and ultimately appropriate *in vivo* studies will be important to establish the formulation's biological performance further.

An important strength of the present study is its integrated formulation-to-biological evaluation of the developed berberine-loaded nanoemulgel. The formulation was assessed through complementary physicochemical and pharmaceutical approaches, including nanoemulsion screening, accelerated-stress testing, TEM-based morphological characterization, rheological and mechanical characterization, three-month storage evaluation, drug-release analysis, *ex vivo* skin permeation and deposition, and keratinocyte-based cytocompatibility and migration assays. This multifaceted approach allowed us to examine the selected formulation's behavior across successive stages of development rather than based on a single formulation attribute. In particular, the combination of sustained berberine release, higher mean skin deposition among the tested formulations, acceptable HaCaT cytocompatibility under the investigated conditions, and enhanced scratch closure relative to free berberine provides complementary evidence supporting its potential as a topical delivery platform.

Despite the strengths of the present study, several limitations should be considered when interpreting the findings. First, encapsulation efficiency and drug-loading capacity were not determined. These parameters are important for quantitatively defining the association of berberine with the nanoemulsion system and for relating formulation composition to drug-release and skin-delivery behavior. Their absence therefore limits a complete quantitative characterization of drug incorporation into the carrier. Future studies should determine encapsulation efficiency and drug loading using validated separation and analytical procedures and examine their relationship with release and cutaneous delivery. In addition, because droplet size in the nanoemulgels was determined by DLS after sample dilution, matrix-dependent changes occurring during dilution may have influenced the measured hydrodynamic size, particularly after thermal stress; therefore, the substantial post-thermal reductions in mean droplet size should be interpreted cautiously.

Second, the *in vitro* release study used a dialysis membrane, which introduces an additional diffusional barrier between the formulation and the release medium. Consequently, the observed release profile may reflect not only drug release from the formulation but also diffusion across the membrane, potentially affecting interpretation of the intrinsic release kinetics. Nevertheless, because all formulations were evaluated using the same membrane and under identical experimental conditions, the method provides a consistent basis for comparing their apparent release behavior. Future studies should characterize membrane-related effects and, where appropriate, employ complementary release methods designed to minimize membrane-controlled diffusion.

Third, although the *ex vivo* skin experiments provided quantitative information on the amount of berberine recovered from the skin and receptor compartment, they did not determine the penetration pathway or spatial localization of berberine within individual skin layers. Therefore, the higher mean skin deposition observed with the nanoemulgel should be interpreted as a quantitative skin-recovery finding rather than direct evidence of enhanced penetration into specific skin layers or of a defined skin-delivery mechanism. In addition, the experimental design did not permit comprehensive characterization of steady-state permeation parameters. These factors limit mechanistic interpretation of the observed skin-distribution pattern and preclude a complete pharmacokinetic description of cutaneous transport. Future studies should therefore include extended permeation experiments to calculate steady-state flux, permeability coefficient, and lag time, along with complementary imaging approaches such as confocal laser scanning microscopy (CLSM) or fluorescence imaging to determine berberine's spatial distribution within the skin and investigate potential penetration pathways.

Fourth, occlusion and skin-hydration effects were not directly evaluated. Because changes in stratum corneum hydration may alter barrier properties and consequently influence topical drug penetration and retention, the present experiments cannot establish the contribution of these formulation-related effects to the observed skin-delivery profile. Future studies should therefore incorporate appropriate measurements of occlusion and skin hydration to clarify their contribution to cutaneous delivery.

Fifth, the biological evaluation was restricted to HaCaT keratinocytes, and fibroblast-based experiments were not performed. Although HaCaT cells provide a useful model for preliminary evaluation of keratinocyte cytocompatibility and scratch closure, wound repair is a multicellular process involving coordinated interactions among keratinocytes, fibroblasts, immune cells, and other cellular components. In particular, dermal fibroblasts contribute to extracellular matrix deposition, wound contraction, and tissue remodeling. Therefore, these HaCaT-based findings cannot establish the nanoemulgel's effects on the fibroblast component of wound repair or be extrapolated to the overall wound-healing response. Moreover, inflammatory biomarkers were not measured, a composition-matched placebo nanoemulgel was not included in the scratch assay,

Corrected Proof

and dedicated topical irritation or local tolerability studies were not performed. Although the formulation showed acceptable cytocompatibility toward HaCaT keratinocytes under the investigated *in vitro* conditions, this finding cannot substitute for a dedicated topical safety assessment and does not establish the formulation's irritation potential or local tolerability after skin application.

Consequently, the present experimental design cannot distinguish berberine's specific contribution from potential effects of formulation excipients on scratch closure, demonstrate an anti-inflammatory mechanism, or establish the topical safety profile of the developed nanoemulgel.

Future investigations should include NIH-3T3 fibroblasts or, preferably, primary human dermal fibroblasts, together with a composition-matched placebo nanoemulgel control, migration-specific assays, inflammatory biomarkers such as TNF-α, IL-6, and IL-1β, co-culture or three-dimensional skin models, validated reconstructed human epidermis-based skin irritation models and other appropriate topical tolerability assessments, and ultimately appropriate *in vivo* wound models.

Finally, this study did not evaluate antimicrobial activity. Therefore, although the literature reports antimicrobial effects of berberine, the present findings do not support conclusions about the antimicrobial performance of the developed nanoemulgel. Future studies may include dedicated antimicrobial and antibiofilm assays, particularly if the formulation is further investigated for infected-wound applications.

Collectively, these limitations indicate that the present findings establish the physicochemical performance, *ex vivo* skin-delivery behavior, cytocompatibility, and *in vitro* scratch-closure potential of the developed nanoemulgel, but do not constitute definitive evidence of *in vivo* wound-healing efficacy.

Conclusion

This study successfully developed a *Q. saponin*-stabilized berberine-loaded nanoemulgel for topical delivery. The optimized formulation (NEJ1.3) exhibited favorable physicochemical characteristics and maintained satisfactory stability during the evaluated storage period. The nanoemulgel exhibited sustained berberine release and the highest mean skin deposition among the tested formulations under the experimental conditions used.

The optimized nanoemulgel also demonstrated acceptable cytocompatibility toward HaCaT keratinocytes under the tested conditions and produced significantly greater *in vitro* scratch closure than free berberine after 24 hr (76.33±3.43% vs. 25.56±4.29%, $P<0.0001$). Collectively, these findings demonstrate the physicochemical and pharmaceutical performance of the developed formulation and provide preliminary keratinocyte-based evidence supporting its further investigation as a topical berberine delivery system for wound-related applications. However, because the biological evaluation was limited to HaCaT keratinocytes and an *in vitro* scratch assay, and because scratch closure reflects cell migration and potentially proliferation, the present findings should not be interpreted as evidence of therapeutic wound-healing efficacy. Further evaluation using fibroblast-based and more complex wound models, followed by appropriate *in vivo* wound-healing studies, is required to establish its therapeutic efficacy and biological relevance. Dedicated topical irritation and local tolerability studies are also required to establish the formulation's safety profile for cutaneous application.

Acknowledgment

This research received no specific grant from any funding agency in the public, commercial, or not-for-profit sectors.

Ethics Approval

Ethical approval was not required because this study involved no experiments with human participants or live animals. The porcine skin used in the *ex vivo* permeation study was obtained as post-mortem tissue from animals slaughtered for reasons unrelated to this research. Therefore, no animals were sacrificed specifically for this study.

Authors' Contributions

E A conceived and designed the study, developed the formulation strategy and methodology, supervised the project, secured the funding required for the study, analyzed and interpreted the data, prepared the original draft of the manuscript, and finalized the manuscript. Z O performed most of the experimental work, collected and processed the data, and contributed to data analysis and interpretation. AG Y conducted the Franz diffusion experiments and helped organize and process the experimental data. E A, Z O, and AG Y approved the final version of the manuscript and agreed to be accountable for all aspects of the work.

Conflicts of Interest

The authors declare no conflicts of interest.

Declaration

The authors acknowledge using ChatGPT (OpenAI) for language editing and to improve the clarity and readability of selected sections of the manuscript during revision. The authors critically reviewed and revised all AI-assisted content and take full responsibility for the manuscript's scientific content and final version.

References

1. Mamun AA, Shao C, Geng P, Wang S, Xiao J. Recent advances in molecular mechanisms of skin wound healing and its treatments. Front Immunol 2024; 15: 1395479.

2. Mirhaj M, Labbaf S, Tavakoli M, Seifalian AM. Emerging treatment strategies in wound care. Int Wound J 2022; 19: 1934-1954.

3. Cedillo-Cortezano M, Martinez-Cuevas LR, López JAM, Barrera López IL, Escutia-Perez S, Petricevich VL. Use of medicinal plants in the process of wound healing: A literature review. Pharmaceuticals (Basel) 2024; 17: 303.

4. Samadian H, Zamiri S, Ehterami A, Farzamfar S, Vaez A, Khastar H, *et al.* Electrospun cellulose acetate/gelatin nanofibrous wound dressing containing berberine for diabetic foot ulcer healing: *In vitro* and in vivo studies. Sci Rep 2020; 10: 8312.

5. Panda DS, Eid HM, Elkomy MH, Khames A, Hassan RM, Abo El-Ela FI, *et al.* Berberine encapsulated lecithin-chitosan nanoparticles as innovative wound healing agent in type II diabetes. Pharmaceutics 2021; 13: 1197.

6. Mayangsari F, Surini S, Iswandana R. Development of transfersomal emulgel to enhance the permeation of berberine chloride for transdermal delivery. J Appl Pharm Sci 2022; 12: 048-055.

7. Kong M, Chen XG, Kweon DK, Park HJ. Investigations on skin permeation of hyaluronic acid based nanoemulsion as transdermal

Corrected Proof

carrier. Carbohydr Polym 2011; 86:837-843.
8.Arya K, Bhar R, Kataria R, Mehta SK. Nanomaterials in the cosmetics industry: A greener approach. Green Nanomaterials for Industrial Applications: Elsevier; 2022. P. 207-253.
9. Hwang J, Park JY, Kang J, Oh N, Li C, Yoo CY, *et al.* Enhanced drug delivery with oil- in- water nanoemulsions: Stability and sustained release of doxorubicin. Macromol Rapid Commun 2024; 45: 2400480.
10. Liao Y, Li Z, Zhou Q, Sheng M, Qu Q, Shi Y, *et al.* Saponin surfactants used in drug delivery systems: A new application for natural medicine components. Int J Pharm 2021; 603: 120709.
11. Fleck JD, Betti AH, Da Silva FP, Troian EA, Olivaro C, Ferreira F, *et al.* Saponins from *Quillaja saponaria* and *Quillaja brasiliensis*: Particular chemical characteristics and biological activities. Molecules 2019; 24: 171.
12. Schreiner TB, Dias MM, Barreiro MF, Pinho SP. Saponins as natural emulsifiers for nanoemulsions. J Agric Food Chem 2022; 70: 6573.
13. Schreiner TB, Santamaria-Echart A, Ribeiro A, Peres AM, Dias MM, Pinho SP, *et al.* Formulation and optimization of nanoemulsions using the natural surfactant saponin from quillaja bark. Molecules 2020; 25: 1538.
14. Sghier K, Mur M, Veiga F, Paiva-Santos AC, Pires PC. Novel therapeutic hybrid systems using hydrogels and nanotechnology: A focus on nanoemulgels for the treatment of skin diseases. Gels 2024; 10: 45.
15. Donthi MR, Munnangi SR, Krishna KV, Saha RN, Singhvi G, Dubey SK. Nanoemulgel: A novel nano carrier as a tool for topical drug delivery. Pharmaceutics 2023; 15: 164.
16. Yeo E, Chieng CJY, Choudhury H, Pandey M, Gorain B. Tocotrienols-rich naringenin nanoemulgel for the management of diabetic wound: Fabrication, characterization and comparative *in vitro* evaluations. Curr Res Pharmacol Drug Discov 2021; 2: 100019.
17. Algahtani MS, Ahmad MZ, Nourein IH, Albarqi HA, Alyami HS, Alyami MH, *et al.* Preparation and characterization of curcumin nanoemulgel utilizing ultrasonication technique for wound healing: *In vitro*, *ex vivo*, and *in vivo* evaluation. Gels 2021; 7: 213.
18. Algahtani MS, Ahmad MZ, Shaikh IA, Abdel-Wahab BA, Nourein IH, Ahmad J. Thymoquinone loaded topical nanoemulgel for wound healing: Formulation design and *in-vivo* evaluation. Molecules 2021; 26: 3863.
19. Schreiner TB, Santamaria-Echart A, Colucci G, Plasencia P, Costa PS, Dias MM, *et al.* Saponin-based natural nanoemulsions as alpha-tocopherol delivery systems for dermal applications. J Mol Liq 2023; 391: 123371.
20. Sugumar S, Singh S, Mukherjee K, Chandrasekaran N. Nanoemulsion of orange oil with non ionic surfactant produced emulsion using ultrasonication technique: Evaluating against food spoilage yeast. Appl Nanosci 2016; 6: 113-120.
21. Silva HD, Cerqueira MA, Vicente AA. Influence of surfactant and processing conditions in the stability of oil-in-water nanoemulsions. J Food Eng 2015; 167: 89-98.
22. Acevedo-Fani A, Silva HD, Soliva-Fortuny R, Martin-Belloso O, Vicente AA. Formation, stability and antioxidant activity of food-grade multilayer emulsions containing resveratrol. Food Hydrocolloids 2017; 71: 207-215.
23. Bernardi DS, Pereira TA, Maciel NR, Bortoloto J, Viera GS, Oliveira GC, *et al.* Formation and stability of oil-in-water nanoemulsions containing rice bran oil: *In vitro* and *in vivo* assessments. J Nanobiotechnol 2011; 9: 44.
24. Maruno M. Characterization and stability studies on vegetable nanoemulsions obtained by low energy process. J Nanomedic Nanotechnol sec 2017; 8: 2.
25. Gonçalves RF, Zhou H, Vicente AA, Pinheiro AC, McClements DJ. Plant-based bigels for delivery of bioactive compounds: Influence of hydrogel: Oleogel ratio and protein concentration on their physicochemical properties. Food Hydrocolloids 2024; 150: 109721.
26. Szymańska I, Żbikowska A, Kowalska M. Physical stability of model emulsions based on ethyl cellulose oleogels. Int Agrophys 2020; 34: 289-300.
27. Shigwan H, Saklani A, Hamrapurkar P, Mane T, Bhatt P. HPLC method development and validation for quantification of berberine from *Berberis aristata* and *Berberis tinctoria*. Int J Appl Sci Eng 2013; 11: 203-211.
28. Panda A, Raikwar A, Panda S. A holistic perspective on analytical method validation under International Council for Harmonisation Q2 (R1). Am J Biopharm Pharm Sci 2025; 5: 1.
29. Desai PR, Marepally S, Patel AR, Voshavar C, Chaudhuri A, Singh M. Topical delivery of anti-TNFα siRNA and capsaicin via novel lipid-polymer hybrid nanoparticles efficiently inhibits skin inflammation *in vivo*. J Control Release 2013; 170: 51-63.
30. Mishra R, Dhole S. Lipid-based floating multiparticulate delivery system for bioavailability enhancement of berberine hydrochloride. J Appl Pharm Sci 2019; 9: 036-047.
31. Silva IR, Lima FA, Reis EC, Ferreira LA, Goulart GA. Stepwise protocols for preparation and use of porcine ear skin for *in vitro* skin permeation studies using Franz diffusion cells. Curr Protoc 2022; 2: e391.
32. Ijaz F, Nasir B, Rashid SA, Naseem F, Jalil A, Riaz A, *et al.* Colistin adorned topical nanoemulsion gel formulation for enhanced anti-microbial activity. Sci Rep 2025; 15: 34064.
33. Wang W, Wat E, Hui PC, Chan B, Ng FS, Kan C-W, *et al.* Dual-functional transdermal drug delivery system with controllable drug loading based on thermosensitive poloxamer hydrogel for atopic dermatitis treatment. Sci Rep 2016; 6: 24112.
34. Dubey P, Kumar V, Vaiphei KK, Basrani S, Jadhav A, Wilen C-E, *et al.* Poly-δ-decalactone (PDL) based nanoemulgel for topical delivery of ketoconazole and eugenol against Candida albicans. Nanoscale Adv 2024; 6: 5322-5336.
35. Sahu P, Kashaw SK, Sau S, Kushwah V, Jain S, Agrawal RK, *et al.* pH responsive 5-fluorouracil loaded biocompatible nanogels for topical chemotherapy of aggressive melanoma. Colloids Surf B Biointerfaces 2019; 174: 232-245.
36. Budama-Kilinc Y, Gok B. Development of phyto-compound-based nanoformulation for skin regeneration and its *in vitro* evaluation. J Drug Deliv Sci Technol 2024; 101: 106250.
37. Maded ZK, Sfar S, Taqa GAA, Lassoued MA, Ben Hadj Ayed O, Fawzi HA. Development and optimization of Dipyridamole- and Roflumilast-Loaded nanoemulsion and nanoemulgel for enhanced skin permeation: formulation, characterization, and *in vitro* assessment. Pharmaceuticals 2024; 17: 803.
38. Ahmad N, Ahmad R, Al-Qudaihi A, Alaseel SE, Fita IZ, Khalid MS, *et al.* Preparation of a novel curcumin nanoemulsion by ultrasonication and its comparative effects in wound healing and the treatment of inflammation. RSC Adv 2019; 9: 20192-20206.
39. Nguyen VH, Nguyen MCN, Nguyen HTT. Berberine nanostructured lipid carriers by ultrasonication technique: initial study for skin and oral administration. Adv Nat Sci Nanosci Nanotechnol 2025; 16: 015002.
40. Bahloul B, Ben Bnina E, Dridi D, Bouhamed A, Castillo Henríquez L, Flamini G, *et al.* Development and investigation of a nanoemulgel formulated from tunisian *Opuntia ficus*-indica l. seed oil for enhanced wound healing activity. Gels 2024; 10: 582.
41. Rehman A, Iqbal M, Khan BA, Khan MK, Huwaimel B, Alshehri S, *et al.* Fabrication, *in vitro*, and *in vivo* assessment of eucalyptol-loaded nanoemulgel as a novel paradigm for wound healing. Pharmaceutics 2022; 14: 1971.
42. Mustafa HM, Mohd Amin NA, Zakaria R, Anuar MS, Baharuddin AS. Effect of gelatin/xanthan gum ratios on jackfruit leaf extract nanoemulsion gel stability and properties. BioResources 2025; 20: 2056-2070.
43. Cortes H, Caballero-Florán IH, Mendoza-Muñoz N, Escutia-Guadarrama L, Figueroa-González G, Reyes-Hernández OD, *et al.* Xanthan gum in drug release. Cell Mol Biol 2020; 66: 199-207.
44. Gethin G. The significance of surface pH in chronic wounds. Wounds uk 2007; 3: 52.
45. Mahdi ZH, Suhail A, Maraie NK, Kathem HS. Variables affecting in-vitro evaluation of loxoprofen sodium topical emulgel.

Corrected Proof

Iraqi J Pharm Sci 2024; 33: 92-100.
46. Patel J, Maji B, Moorthy NHN, Maiti S. Xanthan gum derivatives: Review of synthesis, properties and diverse applications. RSC Adv 2020; 10: 27103-27136.
47. Saab M, Raafat K, El-Maradny hr. Transdermal delivery of capsaicin nanoemulgel: Optimization, skin permeation and *in vivo* activity against diabetic neuropathy. Adv Pharm Bullet 2021; 12: 780.
48. Ghica MV, Hîrjău M, Lupuleasa D, Dinu-Pîrvu C-E. Flow and thixotropic parameters for rheological characterization of hydrogels. Molecules 2016; 21: 786.
49. Mirmasoudi SS, Pourmohammadi-Bejarpasi Z, Shahrousvand M, Roudkenar MH. Xanthan gum hydrogel wound dressing enhances wound healing in a rat excisional injury model. Heliyon 2025; 11: 1-11.
50. Hurler J, Engesland A, Poorahmary Kermany B, Škalko- Basnet N. Improved texture analysis for hydrogel characterization: Gel cohesiveness, adhesiveness, and hardness. J Appl polym Sci 2012; 125: 180-188.
51. Yılmaz Usta D, Teksin ZS, Tugcu-Demiroz F. Evaluation of emulgel and nanostructured lipid carrier-based gel formulations for transdermal administration of ibuprofen: Characterization, mechanical properties, and *ex-vivo* skin permeation. AAPS Pharmscitech 2024; 25: 124.
52. Akhter MH, Al-Keridis LA, Saeed M, Khalilullah H, Rab SO, Aljadaan AM, *et al.* Enhanced drug delivery and wound healing potential of berberine-loaded chitosan–alginate nanocomposite gel: Characterization and *in vivo* assessment. Front Public Health 2023; 11: 1238961.
53. Li J, Mooney DJ. Designing hydrogels for controlled drug delivery. Nat Rev Mater 2016; 1: 1-17.
54. Xu C, He J, Wang Y, Xu Z, Ma X, Meng X. Photodegradation of berberine hydrochloride under simulated sunlight irradiation. J Appl Spectrosc 2020; 87: 958-964.
55. Khoshandam A, Imenshahidi M, Hosseinzadeh H. Pharmacokinetic of berberine, the main constituent of *Berberis vulgaris* L.: A comprehensive review. Phytother Res 2022; 36: 4079.
56. Li Y-J, Hu X-B, Lu X-L, Liao D-H, Tang T-T, Wu J-Y, *et al.* Nanoemulsion-based delivery system for enhanced oral bioavailability and caco-2 cell monolayers permeability of berberine hydrochloride. Drug Deliv 2017; 24: 1868-1873.
57. Mishra KK, Kaur CD. Screening of process variables using Box–Behnken design in the fabrication of berberine hydrochloride-loaded transethosomes for enhanced transdermal delivery. Thai J Pharm Sci 2022; 46: 191-202.
58. Gruber S, Nickel A. Toxic or not toxic? The specifications of the standard ISO 10993-5 are not explicit enough to yield comparable results in the cytotoxicity assessment of an identical medical device. Front Med Technol 2023; 5: 1195529.
59. Kandárová H, Pôbiš P. The "Big Three" in biocompatibility testing of medical devices: implementation of alternatives to animal experimentation-are we there yet? Front Toxicol 2023; 5: 1337468.
60. Balestrin LA, Kreutz T, Fachel FNS, Bidone J, Gelsleichter NE, Koester LS, *et al. Achyrocline satureioides* (Lam.) DC (Asteraceae) extract-loaded nanoemulsions as a promising topical wound healing delivery system: *In vitro* assessments in human keratinocytes (HaCaT) and HET-CAM irritant potential. Pharmaceutics 2021; 13: 1241.
61. Alves A, Miguel SP, Araújo AR, de Jesús Valle MJ, Sánchez Navarro A, Correia IJ, *et al.* Xanthan gum–konjac glucomannan blend hydrogel for wound healing. Polymers 2020; 12: 99.
62. Jadav M, Pooja D, Adams DJ, Kulhari H. Advances in xanthan gum-based systems for the delivery of therapeutic agents. Pharmaceutics 2023; 15: 402.
63. Sun L, Zhang X, Xu M, Zhang F, Tian F, Cui J, *et al.* Berberine downregulates CDC6 and inhibits proliferation via targeting JAK-STAT3 signaling in keratinocytes. Cell Death Dis 2019; 10: 274.
64. Wang Q, Zhang S, Jiang J, Chen S, Ramakrishna S, Zhao W, *et al.* Electrospun radially oriented berberine-PHBV nanofiber dressing patches for accelerating diabetic wound healing. Regen Biomater 2024; 11: rbae063.

Corrected Proof